AD-A125 295 DYNAMIC RESPONSE OF RAMJET INLETS TO DOWNSTREAM PERTURBATIONS(U) MCDONNELL DOUGLAS RESEARCH LABS ST LOUIS MO M SAJBEN ET AL. 31 JAN 83 MDC-Q0784 1/1

UNCLASSIFIED N00014-80-C-0481 F/G 20/4 NL

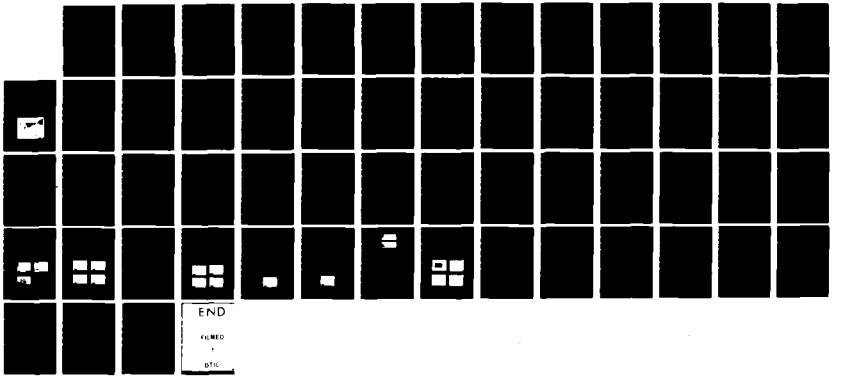

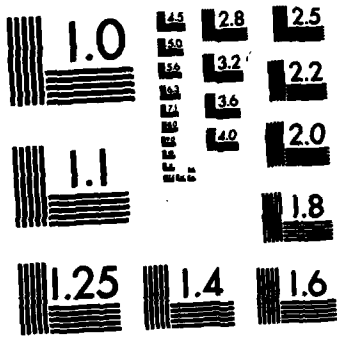

Report MDC Q0784
Contract No. N00014-80-C-0481

DYNAMIC RESPONSE OF RAMJET INLETS TO DOWNSTREAM PERTURBATIONS

M. Sajben
T. J. Bogar
J. C. Kroutil

McDonnell Douglas Research Laboratories
St. Louis, Missouri 63166

31 January 1983
Final Report for Period 1 July 1980 – 31 January 1983

Prepared for:
OFFICE OF NAVAL RESEARCH
800 N. Quincy St.
Arlington, Virginia 22217

MCDONNELL DOUGLAS RESEARCH LABORATORIES

MCDONNELL DOUGLAS CORPORATION

UNCLASSIFIED

SECURITY CLASSIFICATION OF THIS PAGE *(When Data Entered)*

REPORT DOCUMENTATION PAGE

READ INSTRUCTIONS BEFORE COMPLETING FORM

1. REPORT NUMBER: MDC Q0784	2. GOVT ACCESSION NO. A123295
3. RECIPIENT'S CATALOG NUMBER	
4. TITLE *(and Subtitle)*: DYNAMIC RESPONSE OF RAMJET INLETS TO DOWNSTREAM PERTURBATIONS	5. TYPE OF REPORT & PERIOD COVERED: Final Report, 1 Jul 80 - 31 Jan 83
	6. PERFORMING ORG. REPORT NUMBER
7. AUTHOR(s): M. Sajben, T. J. Bogar, J. C. Kroutil	8. CONTRACT OR GRANT NUMBER(s): N00014-80-C-0481
9. PERFORMING ORGANIZATION NAME AND ADDRESS: McDonnell Douglas Research Laboratories, McDonnell Douglas Corporation, P.O. Box 516, St. Louis, MO 63166	10. PROGRAM ELEMENT, PROJECT, TASK AREA & WORK UNIT NUMBERS
11. CONTROLLING OFFICE NAME AND ADDRESS: Office of Naval Research, 800 North Quincy Street, Arlington, VA 22217	12. REPORT DATE: 31 January 1983 13. NUMBER OF PAGES: 55
14. MONITORING AGENCY NAME & ADDRESS *(if different from Controlling Office)*	15. SECURITY CLASS. *(of this report)*: Unclassified 15a. DECLASSIFICATION/DOWNGRADING SCHEDULE

16. DISTRIBUTION STATEMENT *(of this Report)*

17. DISTRIBUTION STATEMENT *(of the abstract entered in Block 20, if different from Report)*

Approved for public release; distribution unlimited

18. SUPPLEMENTARY NOTES

19. KEY WORDS *(Continue on reverse side if necessary and identify by block number)*

Flowfield Oscillations
Air-Breathing Propulsion Systems
Laboratory Simulation Tests
Pressure Fluctuations
Ramjets

20. ABSTRACT *(Continue on reverse side if necessary and identify by block number)*

An external-compression inlet with high-aspect-ratio, rectangular cross sections was investigated in a semi-freejet arrangement at M_∞ = 1.84 and zero incidence, over a wide range of super- and subcritical conditions. The response of the inlet flows to periodic perturbations imposed at the downstream end was determined. The perturbations were created by mechanical modulation of the choked exhaust area at frequencies from 20 to 360 Hz. The amplitude of the pressure fluctuations induced at the downstream end of the

DD FORM 1 JAN 73 1473 EDITION OF 1 NOV 65 IS OBSOLETE

UNCLASSIFIED

SECURITY CLASSIFICATION OF THIS PAGE *(When Data Entered)*

inlet was varied up to 8% of the time-mean static pressure at the same location.

The observed oscillations were categorized according to position ranges associated with the shock motion. Definitions are introduced to clarify often used, but ambiguous, terms relating to criticality, buzz, and unstart.

In supercritical oscillations, the pressure fluctuation amplitudes within the inlet were found to be linearly proportional to the fluctuation intensity at the exit station, establishing the latter as the appropriate quantity for normalization. The normalized pressure fluctuation amplitudes depend on flow condition and frequency; combinations of these leading to maximum fluctuation intensities were determined.

In subcritical conditions, the inlet displays a large-amplitude natural oscillation (buzz). Superimposed excitation may couple with the natural oscillations in two distinctly different ways, both strongly nonlinear.

Combinations of mean flow condition, excitation amplitude, and frequency that cause the terminal shock to move upstream of the cowl or the ramp were determined. The latter occurrence was invariably associated with the onset of large-amplitude buzz. The results show that the supercritical margin required to prevent the onset of buzz increases sharply as the excitation frequency decreases below the natural buzz frequency.

PREFACE

This final report summarizes a research program performed by the McDonnell Douglas Research Laboratories, St. Louis, Missouri, on the response of ramjet inlet flows to periodic downstream disturbances. The disturbances, generated by a mechanical exciter in cold flows, simulate pressure fluctuations that can be exhibited by dump combustor instabilities in tactical-size ramjets. The research was conducted under Contract N00014-80-C-0481 for the Office of Naval Research. The performance period was 1 July 1980 to 31 January 1983.

The principal investigator was Dr. Miklos Sajben; Dr. Thomas J. Bogar and Mr. Joseph C. Kroutil were coinvestigators. The program manager was Dr. Richard S. Miller, Office of Naval Research.

This report has been reviewed and approved.

R. J. Hakkinen
Director-Research
McDonnell Douglas Research Laboratories

D. P. Ames
Staff Vice President
McDonnell Douglas Research Laboratories

TABLE OF CONTENTS

LIST OF ILLUSTRATIONS

LIST OF ILLUSTRATIONS (Continued)

LIST OF TABLES

NOMENCLATURE

A	cross-sectional area
B,E	Fourier coefficients
f	frequency
h	channel height
i,j	dummy indices
M	Mach number
$\tilde{M}$	average Mach number defined by Equation (2)
n	dummy index
p	static pressure
P	rms value of time-dependent pressure; normalized by rms value of exit amplitude
R	perfect gas constant
t	time
T	absolute temperature
u	x-component of velocity vector
x	streamwise (horizontal) coordinate; x = 0 at ramp lip, increasing downstream
y	transverse coordinate; y = 0 at ramp lip, increasing upward
z	spanwise coordinate; zero in plane of symmetry of model
γ	ratio of specific heats
ν_e	pressure ratio (inlet-total/exit-static)
ρ	density

Subscripts

∞	freestream	x-location references
o	cowl lip (geometric throat)	
σ	shock	
e	exit station	
v	choke point at exhaust; approximately coincides with rotor axis	
1,2,3...6	designating orders of harmonics	
c	critical	
b	buzz	
f	narrow-band filtered at excitation frequency	

Superscripts

$\bar{(\ )}$	time-mean
$(\ )'$	time-dependent part
$\hat{(\ )}$	root-mean-square (rms) of time-dependent part
$\tilde{(\ )}$	distance normalized by geometric throat height (h_o = 23.5 mm); except in $\tilde{M}$ (see list of symbols)

1. INTRODUCTION

The liquid-fuel ramjet, combined with an integral solid rocket booster, is a candidate for high-speed tactical missile propulsion systems. The experience of development programs indicates that such systems may display low-frequency (< 300 Hz), large-amplitude (± 15%) pressure oscillations that involve both the combustor and the inlet.[1] If the initial shock system of the inlet is sufficiently disturbed by these fluctuations, the inlet may unstart, resulting in a large reduction of captured airflow and thrust, and eventually causing failure of the mission.

Pressure oscillations in dump-combustor ramjets have been investigated by Hall,[1] Rogers,[2,3] Clark,[4,5] Schadow et al.,[6] Crump et al.,[7] and Waugh et al.[8] One of the widely accepted conclusions of these studies is that the inlet is a significant element of the problem and that the dynamics of inlets require detailed investigation.

The present contract is intended to generate such information through the experimental study of a semi-freejet inlet model subjected to periodic, controlled disturbances at its downstream end, simulating combustor-pressure fluctuations. The disturbances are introduced by the periodic mechanical modulation of the choked exhaust cross-sectional area.

The flow in the same inlet model with steady exit boundary conditions formed the subject of a separate, MDRL-sponsored investigation, in which both time-mean and the time-dependent aspects of the flows were explored. Documentation of the results is available[9]; familiarity with this reference is helpful in understanding the present report.

2. OBJECTIVES

The objectives of this program were contractually stated as follows:

Task I - Design and build an exciter device for periodic modulation of the exhaust area of an appropriate diffuser model.

Task II - Obtain still and motion photographs of unsteady flowfields in a supercritically operated diffuser over suitable combinations of shock strength, excitation frequency, and excitation amplitude.

Task III - Determine unstart boundaries representing combinations of excitation frequency and amplitude that cause the shock to pass through the inlet throat for the available range of terminal shock Mach numbers.

Task IV - Determine phase-averaged shock displacement histories for selected combinations of operating parameters.

3. DESCRIPTION OF EXPERIMENT

3.1 Inlet Model

The original test concept involved a dual-throat model configured as a small supersonic wind tunnel. References to a diffuser in the task statements reflect these initial ideas. However, it soon became clear that the principal objectives would be better served by an inlet model in a semi-freejet arrangement, and the approach was changed accordingly. An inlet model available from an MDC-sponsored investigation was used. The model (Figures 1, 2 and 3) is an external-compression*, ramp-type inlet operated in a semi-freejet mode in the exhaust of a supersonic nozzle. The ramp angle is 14.7^{o}, which in conjunction with the freestream Mach number of 1.84 produces an attached weak oblique shock, yielding a ramp-surface Mach number of 1.3. This Mach number is close to that found in typical ramjet inlets, although it may be produced by a combination of higher freestream Mach numbers and higher ramp angles. The oblique shock is designed to clear the cowl lip by 0.7 mm, such that the cowl lip is also exposed to the post-shock Mach number of 1.3.

The inside surface at the cowl lip is parallel to the flat ramp surface, and the cross-sectional area increases monotonically beyond this point so that a geometric throat ($dh/dx = 0$) is formed at the cowl lip. The height of the channel at this location (h_o = 23.5 mm) is used as a reference length throughout the report. The design makes no allowance for boundary-layer displacement effects on either surface; the flow contains a weak oblique shock (Mach wave) initiated by boundary-layer growth at the cowl lip. The channel continues to diverge (maximum angle is 6.9^{o}) and forms a gradual transition to a constant-area segment. The contours are simple combinations of straight lines and circular arcs; no attempt was made to optimize any performance indicator by tailoring the wall shapes.

*Mixed compression inlets are often used in ramjet technology. They are more efficient at high speeds, but must have variable geometry for starting. The introduction of such requirements into the present study would have diverted a needlessly large fraction of resources from the central issue, and was therefore avoided.

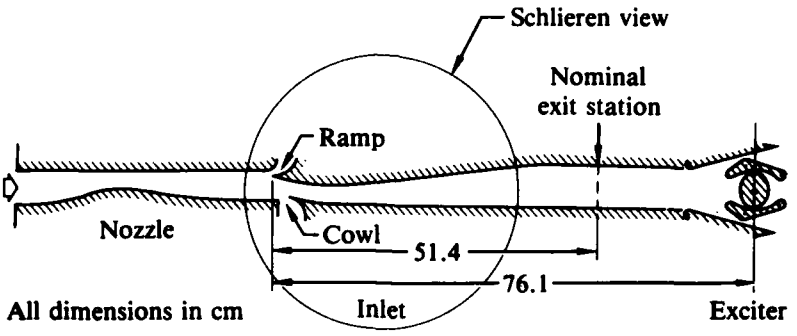

- Inlet and exciter width: 17.78 (constant)
- Aspect ratio at throat: 7.56
  at exit: 2.80

GP31-0114-2

Figure 1. Inlet model including the supersonic nozzle, inlet, and exciter components.

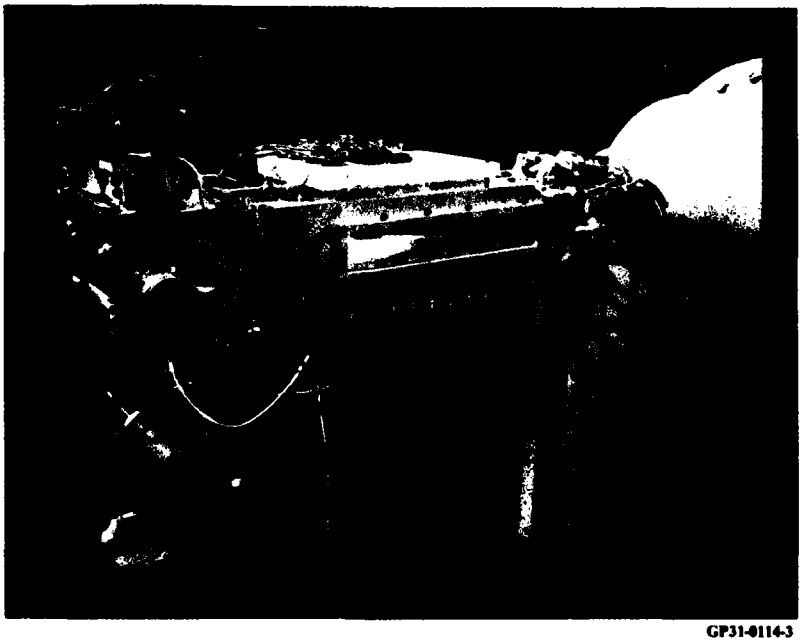

GP31-0114-3

Figure 2. Inlet model installed in test facility.

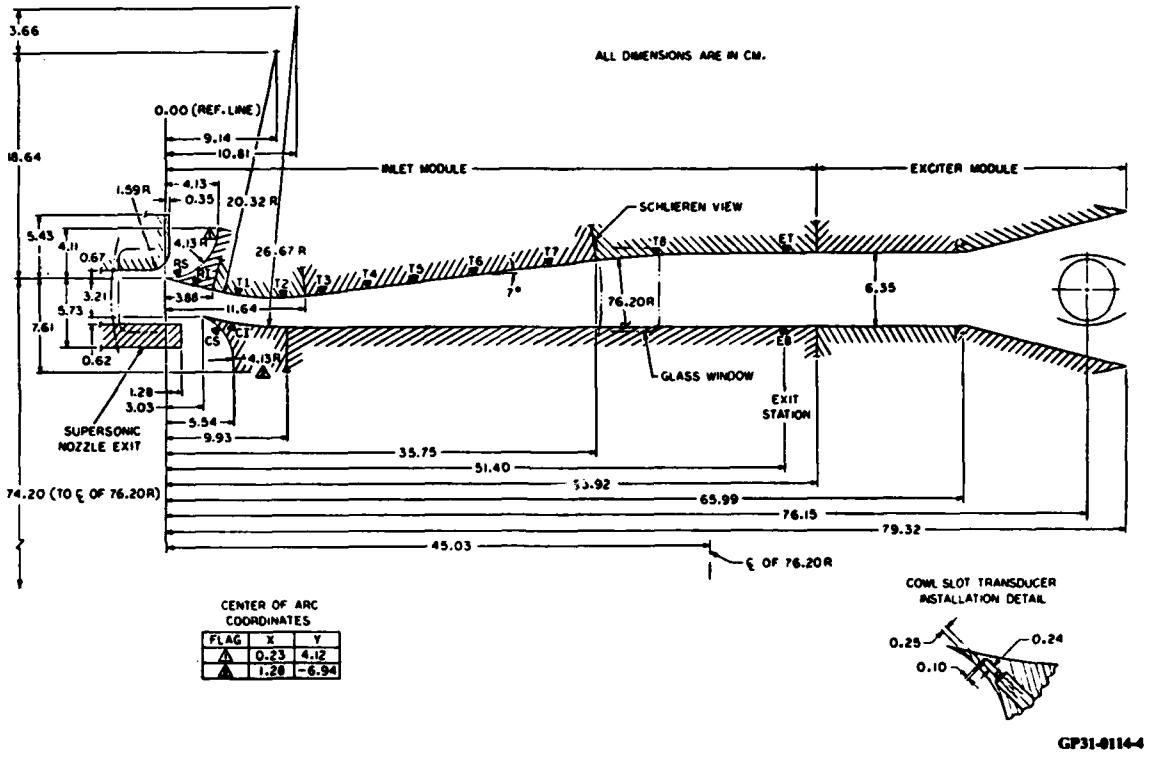

Figure 3. Inlet model contour shapes and locations of fast-response pressure transducers indicated by solid triangles. Origin of the coordinate system is at the ramp lip.

An arbitrarily chosen location within the constant-area terminal segment is designated as the exit station ($\tilde{x}_e$ = 21.91), which serves as the downstream boundary of the flowfield of interest and corresponds to a station just upstream of fuel injection in real ramjets.

The supersonic flow was produced by a two-dimensional, convergent-divergent supersonic nozzle, designed by the method of characteristics and corrected for boundary-layer displacement effects. The inlet is located in the core flow of the nozzle exit; the top and bottom nozzle-wall boundary layers are removed through large slots above and below the ramp and cowl lips, respectively. Approximately 68% of the nozzle flow enters the inlet.

The nozzle is supplied with dry, filtered air from a 51-cm diameter, 160-cm long plenum chamber immediately upstream. The plenum has several flow control screens and a smoothly contoured transition to the nozzle with a contraction ratio of 22.4:1, providing highly uniform, low-turbulence flow. Plenum chamber pressures ranged up to 570 kPa with mass flow rates through the nozzle of 6.7 kg/s.

The nozzle and inlet form a single structural unit with common sidewalls that permit glass windows to overlap the gap between the nozzle and the inlet. This design assures excellent optical access to a region in which important processes occur during start, buzz, and unstart. However, the lack of sidewall boundary-layer control adversely affects two-dimensionality and a large throat aspect-ratio (7.56:1) was chosen to minimize sidewall boundary-layer influence.

3.2 Exciter

Exit area modulation was accomplished by the exciter device shown in Figures 1-4. The principal components of the exciter are an elliptical cross-section rotor with axis horizontal and normal to the flow, two flaps that can be tilted around the indicated hinge points, and two doors formed by the hinged-end segment of the top and bottom walls. These components formed a symmetric arrangement of four parallel flow passages, each shaped as a convergent-divergent channel and choked under all operating conditions.

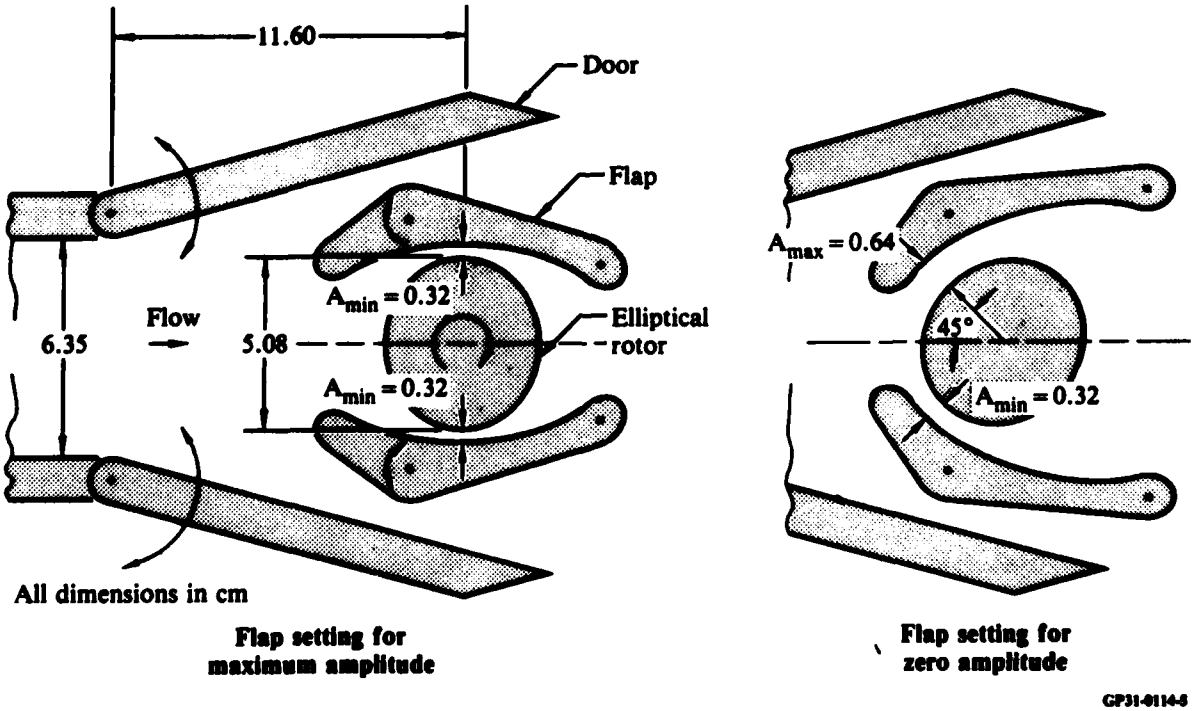

Figure 4. Mechanical exciter and method of amplitude control.

The total cross-sectional area at the choke point (the sum of the four passage areas, referred to as exhaust area) could be varied according to the relation

$$A_v = \bar{A}_v + A_v' \cos(2\pi f_{ex} t) , \qquad (1)$$

where $\bar{A}_v$ is the time-mean value and A_v', f_{ex} are the amplitude and frequency of the time-dependent contribution, respectively. Equation (1) does not describe higher harmonics, which were present with negligible amplitudes only and will not be explicitly considered.

Variation of the three parameters included in the right side of Equation (1) was continuous, noninteracting (or at most weakly interacting), and could be accomplished during runs without shutting down the experiment. The symmetry of the configuration represented an improvement over an asymmetric device used in earlier, similar experiments.[10,11]

The doors and flaps were actuated remotely by appropriate motors and linkages that assured symmetric positioning of the respective component pairs. The rotor was driven by a 0.56 kW variable-speed motor via V-belt pulleys.

The doors fixed the height of the two outer passages, and since the time-mean area of all passages was carefully designed to be independent of flap setting, the time-mean area ($\bar{A}_v$) was determined solely by the door setting. The doors thus performed the control function of the conventional plug throttle commonly used in inlet testing. They were not, however, used for flow measurements as calibrated plugs usually are, for two reasons. First, the exciter assembly was not preceded by a sufficiently long channel segment to create a flow distribution independent of far-upstream events, as would be required for a reliable flow-rate vs. open-area calibration. (Making the channel long would have altered the natural frequencies of the system.) Secondly, the effective time-mean area of the exciter was slightly dependent on excitation amplitude and frequency, introducing additional error sources into any flow measurement attempt. The mean exit area thus did not have a simple connection to mass flow and was therefore considered inappropriate for use as a parameter to characterize time-mean flow conditions.

The rotor modulated the heights of the two inner passages at twice the shaft frequency, with a constant amplitude of 3.18 mm, or 13.5% of the geometric throat height. The amplitude of the modulation was the same for both passages, but the relative phase between the two could be varied by using the flaps. In the flap position shown in Figure 4a, the two areas vary in phase; the minima and maxima occur simultaneously on top and bottom. If the flaps are set as shown in Figure 4b, then the area variations are 180^{o} out of phase, and the occurrence of a minimum on one side is associated with a maximum on the other side. The sum of the two inner passage areas is then constant, and the modulation amplitude (A_v') is zero. Intermediate flap settings produce intermediate amplitudes.

An optical encoder mounted on the rotor shaft provided a pulse train for measurement of the rotor speed and use as a reference in ensemble-averaging various signals. When needed, steady boundary conditions were created by locking the rotor with its major axis horizontal, such that the inner passage areas were maximized.

After an initial development phase, the exciter performed reliably and according to expectations.

3.3 Instrumentation

Fifteen channels of steady data were routinely recorded, including operational variables such as pressures in the plenum chamber and at various locations along the top wall of the nozzle and inlet model, temperatures, and rms values of selected surface pressures.

The top and bottom walls of the model contain over 100 orifices for measuring time-mean wall static-pressure distributions. As shown in Figure 3 and Table 1, 10 ports are located along the top wall, and 2 along the bottom wall, to accommodate sensors for fluctuating surface pressures. Two similar ports, one each in the cowl and ramp slots, were used to detect passage of the terminal shock over the cowl and ramp lips. Miniature strain-gage-type transducers with flat frequency response to 90 kHz were used to measure the unsteady pressures. Surveys of the unsteady wall pressures were amplified, low-pass filtered at 10 kHz, and routed either for recording on FM tape or for further analog signal conditioning.

TABLE 1. FAST-RESPONSE TRANSDUCER LOCATIONS.

Transducer symbol on Figure 3	$\tilde{x}$
Top-wall	
RS (ramp slot)	0.473
RI (ramp inside)	1.035
T1 (top-1)	2.519
T2	4.147
T3	5.761
T4	7.373
T5	8.995
T6	11.114
T7	13.829
T8	17.349
ET (exit top)	21.914
Bottom-wall	
CS (cowl slot)	1.862
CI (cowl inside)	2.348
EB (exit bottom)	21.914

GP31-0114-1

A vertical rake containing four fast-response pressure transducers (1.6 mm o.d.) was used to measure the time-dependent total pressures at the exit station midspan. The rake could be stepped in the vertical direction to three fixed locations, adequately resolving the vertical variation of the unsteady total pressure (12 points).

High-speed (5000 frames/s) schlieren motion pictures were made of the flowfield, with the field-of-view extending from the nozzle exit to $\tilde{x} = 14.6$. Spark photographs were taken with a 10 ns spark source.

4. TEST PARAMETERS

In the absence of excitation, the model displayed a one-parameter family of flows, obtained by adjusting the two exit doors to control the exhaust area ($\bar{A}_v$). The parameter characterizing members of this family was chosen to satisfy the unusual requirements of this experiment.

The conventional parameter choice is the time-mean exhaust area since it is directly related to the inlet mass flow and varies monotonically throughout the available range of flow conditions. Unfortunately, the present, unusual throttling arrangement could not be used reliably to measure the mass flow, for reasons explained in Section 3.2.

The ratio of the time-mean freestream total and exit static pressures (ν_e) is a conceptually sound parameter that could be precisely measured and has been used successfully in earlier work on supercritical diffuser flows.[9,10] However, in the present inlet configuration, ν_e becomes nonunique and therefore of limited value. When the shock is located at the cowl lip, ν_e reaches a minimum. Values greater than the minimum are ambiguous; they may designate conditions with the mean shock position either before or after the cowl lip. Since this study is focused on phenomena centered around just this range of ambiguity, ν_e was not appropriate for the present work.

The exit station Mach number (M_e) had the fewest disadvantages and was adopted as the principal parameter. According to one-dimensional isentropic gas dynamics, M_e varies monotonically with $\bar{A}_v$ and is thus free of the ambiguity problem associated with ν_e. M_e uniquely defines ν_e, but the inverse relation is double-valued.

Since the flow at the exit station was nonuniform, an average Mach number ($\tilde{M}_e$) was defined from midspan profiles of time-mean flow properties as

$$(\tilde{M}_e)^2 = \frac{\int \bar{\rho}(\bar{u})^3 dy}{\gamma R \int \overline{\rho u}\ \bar{T} dy} . \qquad (2)$$

The use of this definition is justified by its close connection to the integral energy balance for the model. If an integral energy equation is written for a control volume enclosed by the model and bounded by a plane sur-

face at the exit station, then the surface integral associated with the exit flow contains two terms, representing the kinetic and thermal energy fluxes. $\tilde{M}_e^2$, as defined by Equation (2), is proportional to the ratio of those two terms. (The factor of proportionality is $2/(\gamma - 1)$.) This definition was preferred to a simple average of $M_e(y)$, which cannot be directly associated with integral considerations.

Local Mach numbers at the exit station were determined from time-mean total pressure data from a fixed, 12-tube rake located at midspan and from the time-mean wall static pressure obtained as the average of four orifices located at the same station.

$\tilde{M}_e$ was based on midspan data only and is greater than the area-average Mach number by varying amounts because of sidewall boundary-layer presence. This discrepancy was accepted because the measurement of Mach number distributions over the entire exit area would have been prohibitively time-consuming. The discrepancy is a measure of deviation from two-dimensionality.

When excitation is used, the amplitude and frequency of the perturbation must also be characterized.

The excitation frequency (f_{ex}) was determined by the exit-area modulation, occurring at twice the rotor shaft frequency. The output from the shaft-mounted encoder provided a pulse train that was counted over fixed time-intervals to yield a precise measurement of f_{ex}.

The intensity of excitation was measured by the exit amplitude ($\hat{p}_{ef}$), defined as the rms value of the narrow-band-filtered wall static pressure signal at the exit-station top wall. The filter center frequency was slaved to the encoder output from the exciter; the band-width was 10 Hz.

The exit amplitude could be varied continuously through the variation of exhaust-area modulation amplitude by positioning the exciter flaps. Five flap settings were selected to cover the available range of amplitudes. In addition to zero and maximum modulation, three intermediate settings were selected so that at $\tilde{M}_e = 0.425$ and $f_{ex} = 350$ Hz, the respective $\hat{p}_{ef}$ values were 0.75, 0.5, and 0.25 of the maximum value. If $\tilde{M}_e$ and f_{ex} differed from this arbitrary choice, then the $\hat{p}_{ef}$ values obtained at the five flap settings generally did not form such a simple arithmetic sequence.

The flaps could be reset to within 0.05 mm, although such accuracy was not required since the parameter of interest, $\hat{p}_{ef}$, was always independently measured.

The pressure ratio (ν_e) is an easily measured mean flow parameter. Knowledge of its dependence on the parameters chosen for this work may be useful in relating the present results to other investigations and is given in Figure 5. (For later convenience, the reciprocal of ν_e is used in the figure.) The principal connection is between ν_e and $\tilde{M}_e$, but the excitation frequency and exit amplitude also have significant effects. Figure 5 also illustrates that a given ν_e may be associated with two $\tilde{M}_e$ values, representing two different flowfields.

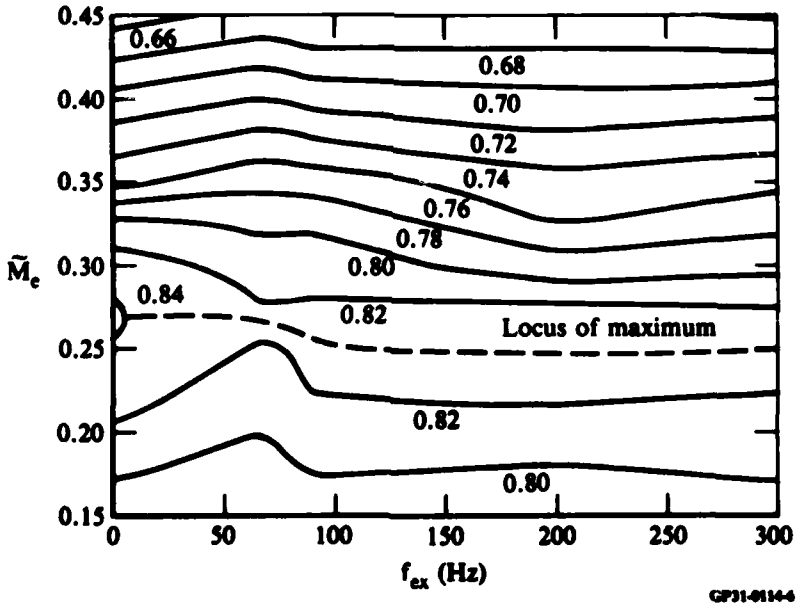

Figure 5. Dependence of normalized exit pressure (p_e/p_{t_∞}) on $\tilde{M}_e$ and f_{ex}, for constant, maximum flap setting.

5. TERMINOLOGY

Ambiguities and conflicting usage of terms concerning inlet flowfields are common in the literature. To avoid misinterpretation, the terminology used in this report will be defined in detail at the outset, specifically considering the experimental fact that the observed inlet flows were never completely steady. Existing conventions will be followed whenever possible.

5.1 Instantaneous Flow States

Classification of the instantaneous flowfields will be based on the streamwise location of the terminal shock (Figure 6). The terminal shock is shown as a single, nominally normal shock, possibly with bifurcated terminations at the walls.

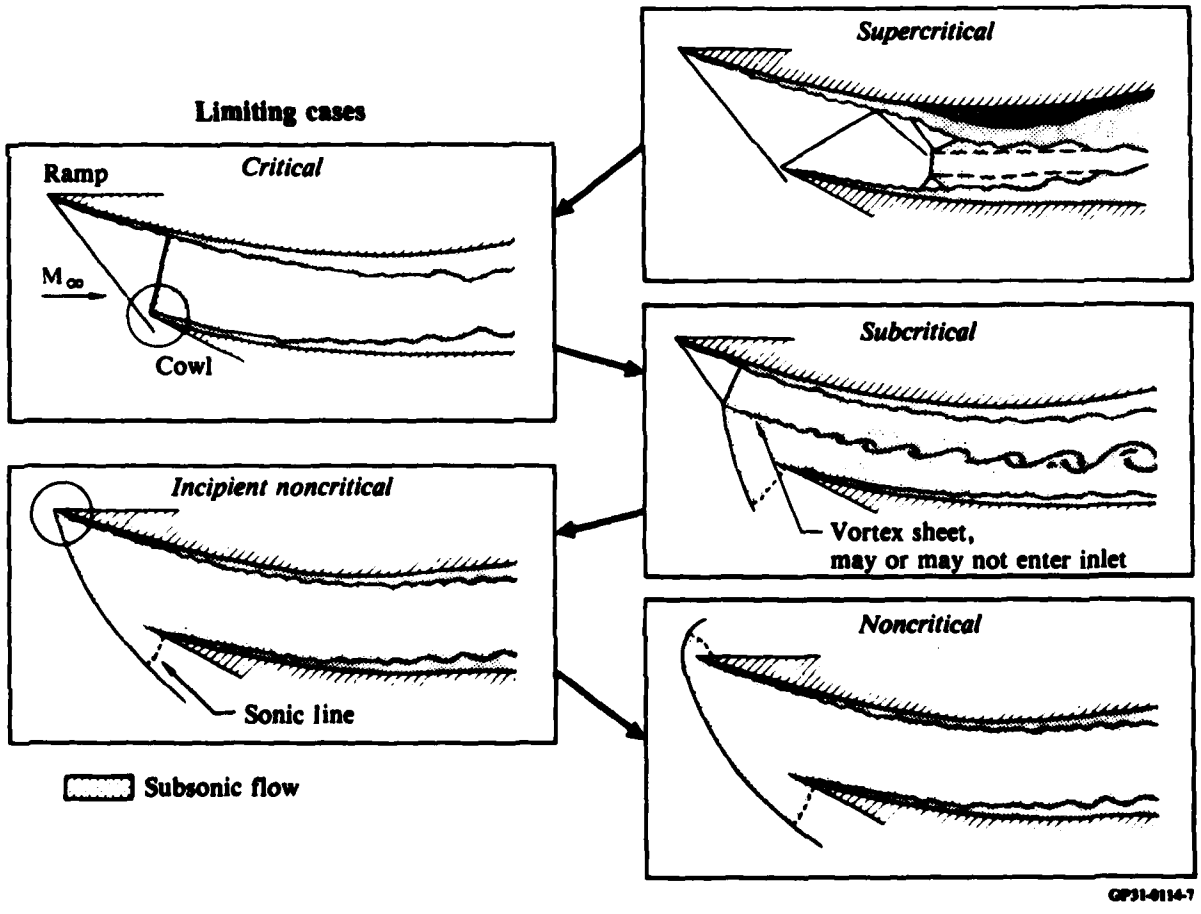

Figure 6. States of criticality for instantaneous inlet flows. Arrows indicate decreasing exhaust area.

The flow is said to be in the supercritical state if the terminal shock is downstream of the cowl lip, subcritical if it is between the ramp and cowl lips, and noncritical if ahead of the ramp lip. Singular states occur if the shock is exactly at the cowl lip (critical) or exactly at the ramp lip (incipient noncritical). The conventional usage considers noncritical states as part of the subcritical range; the distinction introduced here is justified by significant qualitative differences between subcritical and noncritical flows.

In certain circumstances the supersonic/subsonic deceleration in inlets may occur not through a simple normal shock, but across a complex structure of several normal shocks in series (shock train). In such cases, the term "shock position" becomes ambiguous, and the above classification may need to be modified to accommodate the added complications. In the present experiments, shock trains were not observed near singular states.

5.2 Time-Mean Flow Conditions

Since natural oscillations are invariably present, any time-mean flow condition (fixed $\tilde{M}_e$) involves a range of shock positions. Figure 7 illustrates the peak-to-peak ranges found in the present model. The plot shows that some $\tilde{M}_e$ values may be associated with more than one type of criticality, e.g., $\tilde{M}_e = 0.265$ is associated with a shock range that includes both super- and subcritical states.

It is customary and convenient to associate time-mean parameters with a specific criticality. This association will be based on the state assumed by the terminal shock in its upstream-most position. In the above cited example the shock is subcritical in its upstream-most position, and therefore the flow condition defined by $\tilde{M}_e = 0.265$ is called subcritical. Figure 7 illustrates the three time-mean criticality ranges in terms of $\tilde{M}_e$, in accordance with the present convention.

One might consider the time-mean shock position as a basis for the definition of time-mean criticality; however, as will be elaborated later, important qualitative changes of behavior tend to be keyed to the upstream-most shock position. Also, experimental determination of the upstream-most position is simpler, especially with solid sidewall inlet models which offer no optical access to the flow interior.

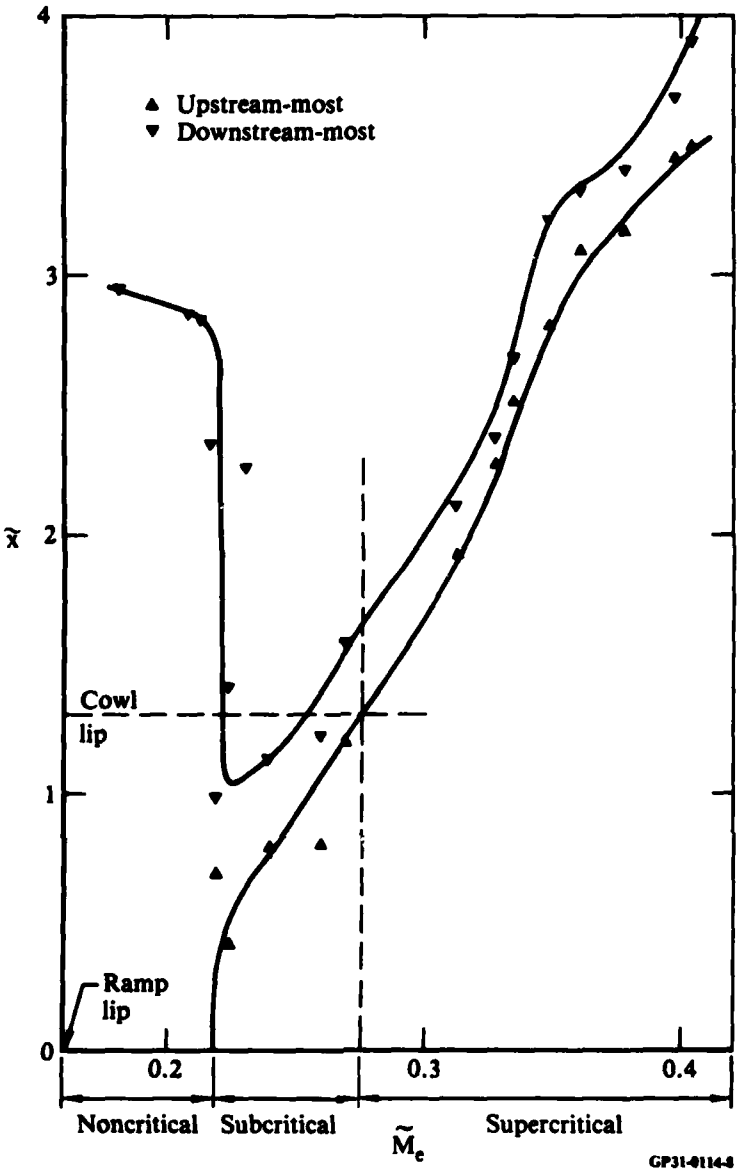

Figure 7. Shock position extremes without excitation and ranges of criticality for time-mean flow conditions.

5.3 Oscillation Modes

The flow exhibited a variety of complex oscillations which may be characterized in different ways. One simple, purely kinematic classification is based on shock position ranges assumed during the motion.

Oscillations in which the instantaneous flow patterns remain in the same class of criticality will be called pure super-, sub-, or noncritical oscillations. Oscillations involving two adjacent criticality ranges are also possible and have been observed (Figure 7, $0.255 < \tilde{M}_e < 0.276$). These will be called dual modes, with the additional qualifiers of super/sub (or sub/non), if the range needs to be described more precisely.

Oscillations may also encompass all three ranges of criticality (Figure 7, $\tilde{M}_e < 0.22$) in which case the oscillation is labeled a triple mode.

The above definitions of oscillation modes do not depend on the cause of the motion and are therefore applicable to both natural and forced oscillations.

5.4 Buzz

The term buzz has been used in the literature to describe many types of inlet oscillations; therefore, it conveys little specific information other than the oscillations are sustained spontaneously and the amplitudes vary from moderate to large.

We use the term buzz to describe oscillations in which periodic changes of instantaneous criticality occur. This includes the dual and triple modes. The triple mode will be alternately and equivalently referred to as full buzz, since in this mode the oscillation amplitudes were much greater than in any of the other modes.

5.5 Unstart

Unstart is defined as a process of a single transition into a condition that is noncritical in both the time-mean and instantaneous sense. This definition implies that the oscillations after the transition (if any) are purely noncritical. The inlet remains in this condition until some externally induced change occurs in the boundary conditions. The initial flow condition and the initial oscillation may be of any type (other than noncritical).

In contrast to buzz, whose definition is based on changes of instantaneous flow states, unstart is defined primarily as a change of time-mean condi-

tions. Full buzz, or dual (sub/non) buzz is thus not to be viewed as a periodic succession of unstarts since no sustained changes of time-mean flow conditions are involved.

5.6 Criticality Boundaries

The terminology established in this section necessitates a reinterpretation of Task III outlined in Section 2. The task statement describes the boundary between super- and subcritical flow conditions and refers to it as unstart boundary. This usage is inconsistent with Section 5.5 and will be remedied as follows:

The set of flow conditions intermediate between two adjacent conditions of time-mean criticality will be referred to as criticality boundaries. There are two such boundaries: the critical boundary (CB) corresponding to the limiting case between the super- and subcritical conditions, and the incipient noncritical boundary (INB) separating the subcritical and noncritical conditions. The boundaries are defined in terms of the three time-mean parameters ($\tilde{M}_e$, f_{ex}, and $\hat{p}_{ef}$) and are themselves time-mean entities.

Because of the definitions introduced in the preceding sections, Task III is reinterpreted to imply the determination of the above two criticality boundaries.

The term unstart boundary (UB) is logically reserved to designate the set of flow conditions causing unstart in the sense of Section 5.5. The determination of UB was not possible in the present experiment because noncritical shock patterns were dominated by the nozzle exit configuration and did not resemble the detached shock pattern expected to exist in an unconfined freestream (Figure 6). The reliable determination of UB requires a wind tunnel test or possibly a free jet experiment with a large jet diameter compared to the model size.

6. UNEXCITED FLOWS

Reference 9 describes in detail the behavior of the inlet model with steady exit boundary conditions. A brief summary of this work is included here for completeness.

The procedure for operating the model was to open the doors fully and pressurize the plenum sufficiently (at least 520 kPa) to cause the initially formed shock system to be swallowed by the inlet. The doors were subsequently adjusted to reach the desired operating condition. The terminal shock moved upstream as the door was closed; it could be located anywhere within the inlet, and driven completely into the nozzle by closing the doors sufficiently.

The present contract work covered all three ranges of criticality, from noncritical conditions ($\tilde{M}_e = 0.12$) to moderate supercriticality ($\tilde{M}_e = 0.42$). In terms of a commonly used engineering definition of supercriticality, $[(\bar{p}_{ec} - \bar{p}_e) / \bar{p}_{ec}]$, the maximum supercriticality was 18%.

6.1 Time-Mean Behavior

For the range of flow conditions investigated, the flow was symmetric with respect to the geometric center plane and possessed a reasonably two-dimensional central region. Figure 8 shows Mach number distributions at the exit station (obtained in the study of Reference 9), deduced from data obtained with a traversable, 12-pronged total-pressure rake. Two-dimensionality is expected to deteriorate in the streamwise direction, so that the illustrated distributions represent the worst case for each flowfield. There was no clear evidence of flow separation in the oil flow traces taken on either the top or bottom wall for $\tilde{M}_e < 0.4$.

The top- and bottom-wall static-pressure distributions are displayed in Figures 9a and 9b. For Figure 9a, the flow is fully supercritical, and in Figure 9b the flow proceeds from critical to noncritical conditions. The supercritical, bottom-wall distributions suggest the presence of shock-induced separation by abrupt changes of slope immediately behind the shock ($\tilde{x} \approx 3$) for $\tilde{M}_e > 0.3$ (compare with Figure 9, Reference 12). This observation is in apparent conflict with the absence of separation as indicated by oil flow traces. Since oil patterns represent time-mean information, the presence of a separation bubble may have been obscured by the large amplitude oscillations,

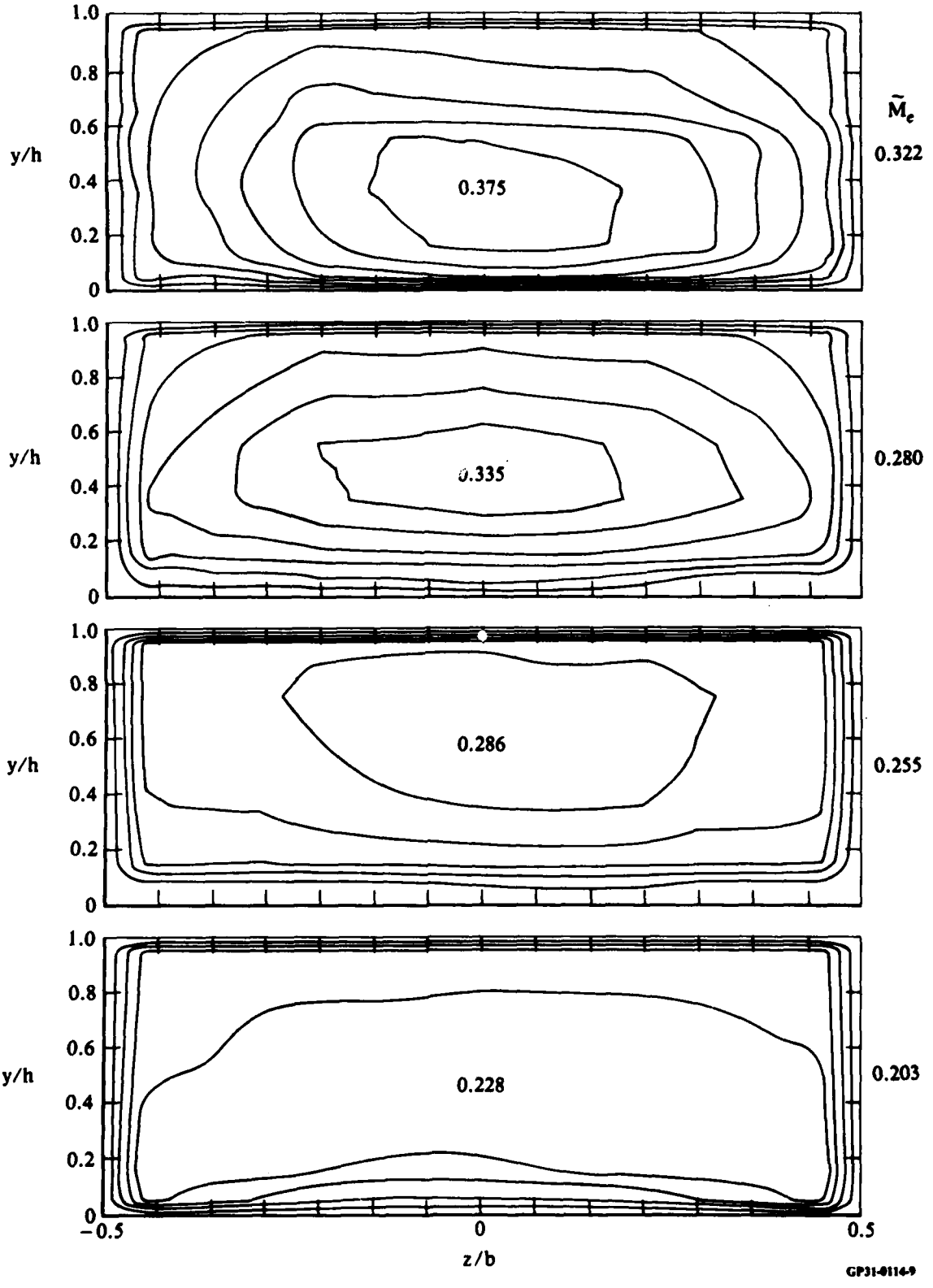

Figure 8. Exit station Mach number contours. Inscribed numbers designate peak values over cross section.

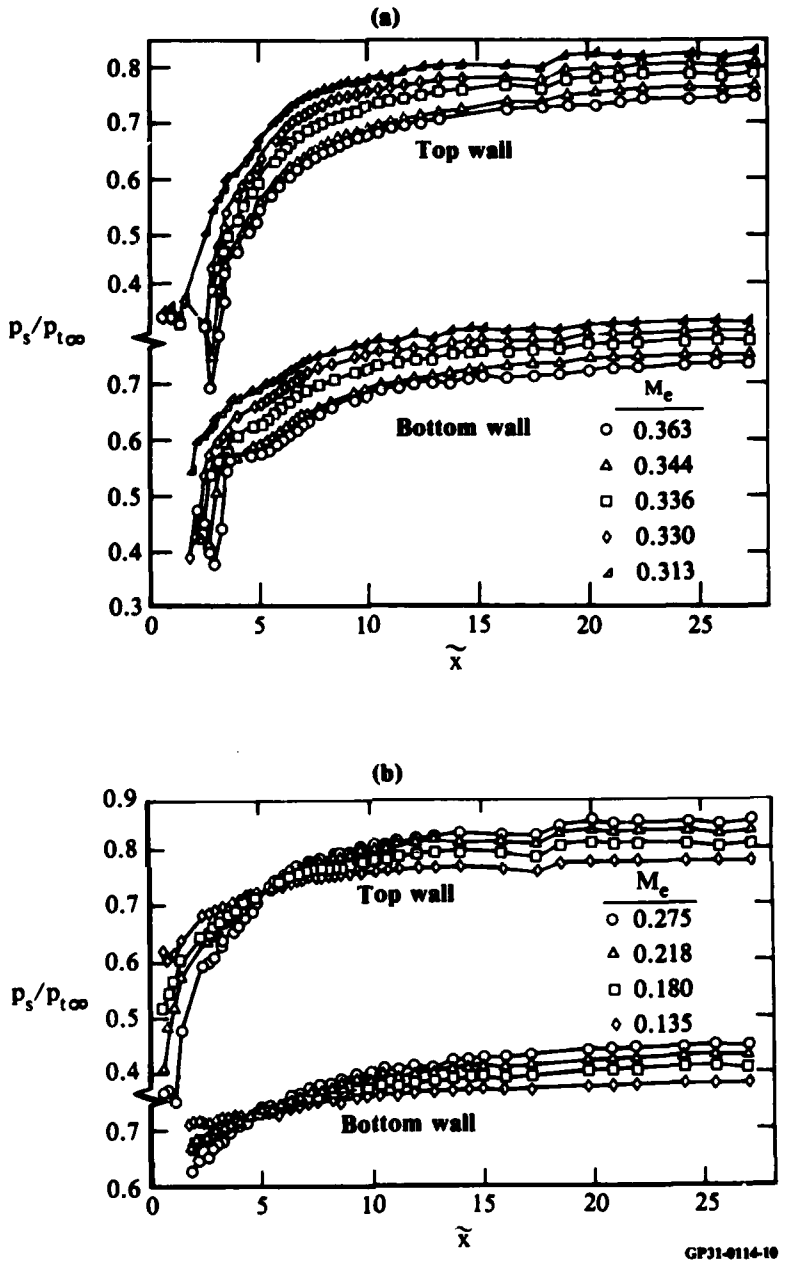

Figure 9. Wall pressure distributions; (a) supercritical and (b) critical and subcritical.

especially if the bubble was small. Separation is not suggested by the bottom-wall pressure distributions for subcritical conditions, or for the top wall under any conditions. This result is unexpected because the terminal shock Mach number (M_σ) is considerably greater than 1.3, the value thought to represent an approximate threshold for incipient shock-induced separation.[10-12] No explanation is presently available.

6.2 Natural Oscillations

As illustrated in Figure 7, the inlet exhibited natural oscillations under all conditions. Pure supercritical and subcritical oscillations as well as a dual (super/sub) mode were found to exist. When the inlet was at the INB boundary, a minute additional closing of the doors caused the inlet to go into full buzz (triple mode), i.e., noncritical conditions were invariably associated with full buzz. No pure noncritical and no sub/non dual modes were observed, probably because of the proximity of the nozzle exit, which strongly influenced the shock pattern displayed by the inlet in noncritical states.

Supercritical oscillations appear to be strongly affected by shock/boundary-layer interactions. The oscillations are random, although the power spectral density distributions of pressures may indicate one or two broad peaks.

Oscillations in which the shock moves ahead of the cowl lip (even if temporarily) tend to be strictly periodic and display a spectrum composed of a set of sharp peaks extending up to six significant harmonics. The fundamental frequency was near 65 Hz. In all these cases, the vortex sheet generated by the bifurcation point (formed by the ramp shock and the terminal shock) is a significant feature of the flow. The vortex sheet is ingested by the inlet and develops into a shear layer that broadens to nearly half of the channel height by $\tilde{x} \cong 16$.

Further details on natural oscillations can be found in Reference 9.

7. EXCITED FLOWS

In a real ramjet, downstream perturbations are introduced by combustion instabilities in the burner where the burning depends on the spatial pressure/velocity distributions of the flow entering the combustor. The inlet and burner oscillations are coupled: any perturbation of the entering flow changes the combustion process, which in turn changes the downstream boundary conditions for the inlet, thereby reacting back to the inlet flow. A theoretical description of this process requires the ability to predict the response of the inlet to downstream boundary conditions and the response of the combustor to the entering flow properties. The present program isolates and focuses on the first of these two problems.

In the present experiments, the combustion instabilities are simulated by modulation of the exit area independently of the response evoked from the inlet. This situation differs from the interactive oscillations in ramjets with combustion; nevertheless, the two systems can be compared meaningfully if interest is confined to the inlet portions. The separation of the inlet from the combustor requires a somwewhat arbitrary definition of a boundary surface separating the two. In the present experiment, the downstream boundary of the inlet was set arbitrarily at $\hat{x}_e = 21.91$ (exit station). If the inlet geometry and the upstream boundary conditions are given (as they will be throughout this report), then specificaton of the time-dependent exit pressure (or, if nonuniform, the distribution of exit pressure) completely defines the entire inlet flow. The manner in which the exit pressure variation is created is immaterial, and a mechanically excited flow is identical to a combustor-excited flow, provided the histories of exit station conditions are identical.

Operation of the exciter created periodic perturbations of all flow properties. The perturbations propagated upstream at the speed of sound with respect to the fluid. These perturbations triggered complex responses from all points of the inlet that either propagated or were convected downstream. The perturbation pressure at the exit station is the sum of the original perturbation and the net result of all local responses; the two contributions cannot be separated in a steady oscillation. The measured exit station perturbations thus should not be thought of as inputs; they represent the input

plus the output returned by the system. For this reason, $\hat{p}_{ef}$ is deliberately called the exit amplitude in preference to the possibly misleading term excitation amplitude.

The time-dependent part of the measured flow quantities contained periodic contributions introduced by the exciter and random contributions from turbulent fluctuations. Interest was focused on the first harmonic of the periodic contribution, obtained by narrow-band filtering of the respective signals at the excitation frequency.

The parameters of the three-dimensional test-matrix were the exit Mach number ($\tilde{M}_e$), the excitation frequency (f_{ex}) and the exit (rms) amplitude ($\hat{p}_{ef}$). This set is reasonably independent of facility-related effects, uniquely characterizes the flow, and is acceptable as input to theoretical considerations. The experimental control of these parameters, however, was neither direct nor independent.

The excitation frequency was the only variable that could be set to any desired value independently of the other two parameters by controlling the rotor speed. In contrast, $\hat{p}_{ef}$ depended strongly on the setting of all three controls: rotor speed, doors, and flaps. $\tilde{M}_e$ depended primarily on the door setting, but rotor speed and flap setting also had nonnegligible influences (Figure 5).

The ideal method of executing a test series having three parameters is to compose it of sub-series in each of which two variables are held constant and only the third is varied. In a three-dimensional parameter-space, the points representing the test-conditions would then lie on straight lines parallel to the axes. Because of the indirect control of the test parameters in the present experiment, there was concurrent variation of at least two independent variables, so that the representative points of a sub-series generally formed a two-dimensional (and sometimes even three-dimensional) curve in the parameter space. Therefore, interpolation is usually necessary to present the data in graphic form.

Time and cost constraints placed severe limitations on the achievable parametric resolution. Ten values for each of the three parameters represent a relatively crude resolution, yet imply a massive test schedule of a thousand runs. Considering that 17 time-dependent flow properties could be measured,

the results would be recorded as 17 000 time traces. The complete exploration of all properties as functions of all parameters over their full ranges is thus not feasible. Judgements and choices were made in defining the test schedule, attempting to focus on the most critical phenomena.

The mode of oscillation occurring at a specific flow condition could be determined reliably from high speed films. The potentially possible oscillatory modes (defined in Section 5.3) are the same with and without excitation, but the actually occurring modes depended on exit amplitude. Figure 10 illustrates the shock position ranges observed during forced oscillations as functions of $\tilde{M}_e$, superimposed on a plot of natural oscillation ranges. All forced oscillation data in the plot were taken with the flaps at maximum setting. The amplitudes are greater by as much as an order-of-magnitude when excitation is present. One consequence of the large amplitudes is that purely subcritical oscillations were not found; only pure supercritical, sub/super dual, and full buzz modes exist.

Figure 10 illustrates that excitation enlarges the shock position ranges at a given value of $\tilde{M}_e$ mostly by extending them downstream, while the upstream-most extreme moves upstream by only a small amount. The time-mean shock position moves downstream by up to two throat heights, i.e., the presence of excitation has the same effect on the mean flow condition as would an increase of exhaust area.

An alternative way of expressing this observation is to state that if the time-mean shock position is kept constant, then the imposition of forced oscillations reduces the associated $\tilde{M}_e$. The unexcited, time-mean inlet characteristics are such that lower $\tilde{M}_e$ is associated with lower total-pressure losses in the subsonic region, suggesting that forced oscillations alleviate subsonic loss mechanisms. No explanation is available at present for this apparent trend.

plus the output returned by the system. For this reason, $\hat{p}_{ef}$ is deliberately called the exit amplitude in preference to the possibly misleading term excitation amplitude.

The time-dependent part of the measured flow quantities contained periodic contributions introduced by the exciter and random contributions from turbulent fluctuations. Interest was focused on the first harmonic of the periodic contribution, obtained by narrow-band filtering of the respective signals at the excitation frequency.

The parameters of the three-dimensional test-matrix were the exit Mach number ($\tilde{M}_e$), the excitation frequency (f_{ex}) and the exit (rms) amplitude ($\hat{p}_{ef}$). This set is reasonably independent of facility-related effects, uniquely characterizes the flow, and is acceptable as input to theoretical considerations. The experimental control of these parameters, however, was neither direct nor independent.

The excitation frequency was the only variable that could be set to any desired value independently of the other two parameters by controlling the rotor speed. In contrast, $\hat{p}_{ef}$ depended strongly on the setting of all three controls: rotor speed, doors, and flaps. $\tilde{M}_e$ depended primarily on the door setting, but rotor speed and flap setting also had nonnegligible influences (Figure 5).

The ideal method of executing a test series having three parameters is to compose it of sub-series in each of which two variables are held constant and only the third is varied. In a three-dimensional parameter-space, the points representing the test-conditions would then lie on straight lines parallel to the axes. Because of the indirect control of the test parameters in the present experiment, there was concurrent variation of at least two independent variables, so that the representative points of a sub-series generally formed a two-dimensional (and sometimes even three-dimensional) curve in the parameter space. Therefore, interpolation is usually necessary to present the data in graphic form.

Time and cost constraints placed severe limitations on the achievable parametric resolution. Ten values for each of the three parameters represent a relatively crude resolution, yet imply a massive test schedule of a thousand runs. Considering that 17 time-dependent flow properties could be measured,

the results would be recorded as 17 000 time traces. The complete exploration of all properties as functions of all parameters over their full ranges is thus not feasible. Judgements and choices were made in defining the test schedule, attempting to focus on the most critical phenomena.

The mode of oscillation occurring at a specific flow condition could be determined reliably from high speed films. The potentially possible oscillatory modes (defined in Section 5.3) are the same with and without excitation, but the actually occurring modes depended on exit amplitude. Figure 10 illustrates the shock position ranges observed during forced oscillations as functions of $\tilde{M}_e$, superimposed on a plot of natural oscillation ranges. All forced oscillation data in the plot were taken with the flaps at maximum setting. The amplitudes are greater by as much as an order-of-magnitude when excitation is present. One consequence of the large amplitudes is that purely subcritical oscillations were not found; only pure supercritical, sub/super dual, and full buzz modes exist.

Figure 10 illustrates that excitation enlarges the shock position ranges at a given value of $\tilde{M}_e$ mostly by extending them downstream, while the upstream-most extreme moves upstream by only a small amount. The time-mean shock position moves downstream by up to two throat heights, i.e., the presence of excitation has the same effect on the mean flow condition as would an increase of exhaust area.

An alternative way of expressing this observation is to state that if the time-mean shock position is kept constant, then the imposition of forced oscillations reduces the associated $\tilde{M}_e$. The unexcited, time-mean inlet characteristics are such that lower $\tilde{M}_e$ is associated with lower total-pressure losses in the subsonic region, suggesting that forced oscillations alleviate subsonic loss mechanisms. No explanation is available at present for this apparent trend.

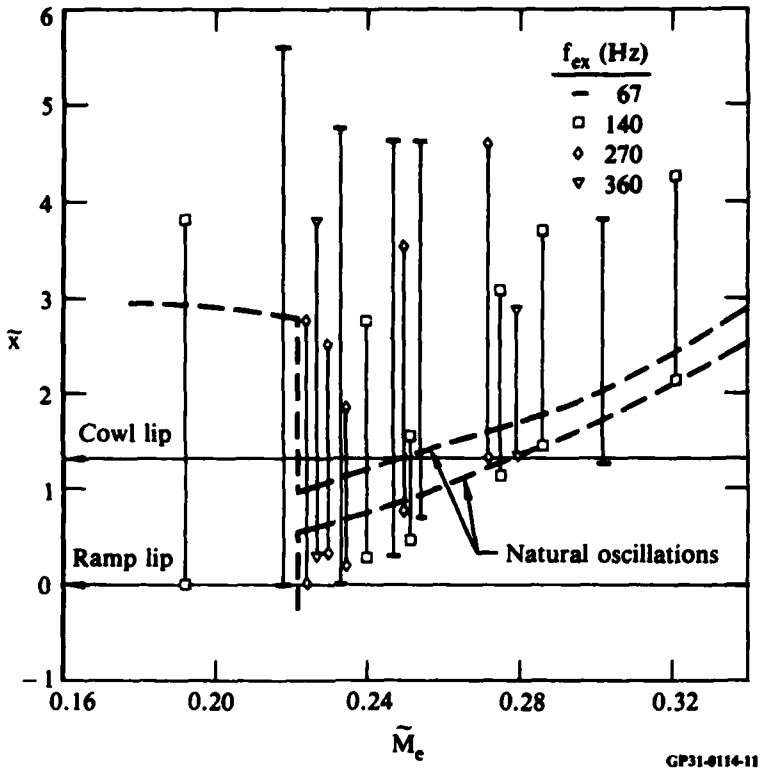

Figure 10. Shock position extremes for forced oscillations with maximum flap setting. Extremes for natural oscillations are also shown for comparison.

7.1 Supercritical Oscillations

In this class of motions the shock always stayed downstream of the cowl, the flow at the geometric throat was always steady, and the mass flow into the inlet was constant. These conditions combined to create a relatively simple type of motion.

Figure 11 illustrates how the exit amplitude varies with excitation frequency if the flap setting is held constant. The concurrent variation of the two principal parameters is evident. Results from (filtered) wall pressure transducers located at interior points yield similar plots, but with major differences in the locations and magnitudes of the minimum or maximum values. In light of the concurrent variation of f_{ex} and $\hat{p}_{ef}$, it is difficult to separate the frequency and amplitude effects.

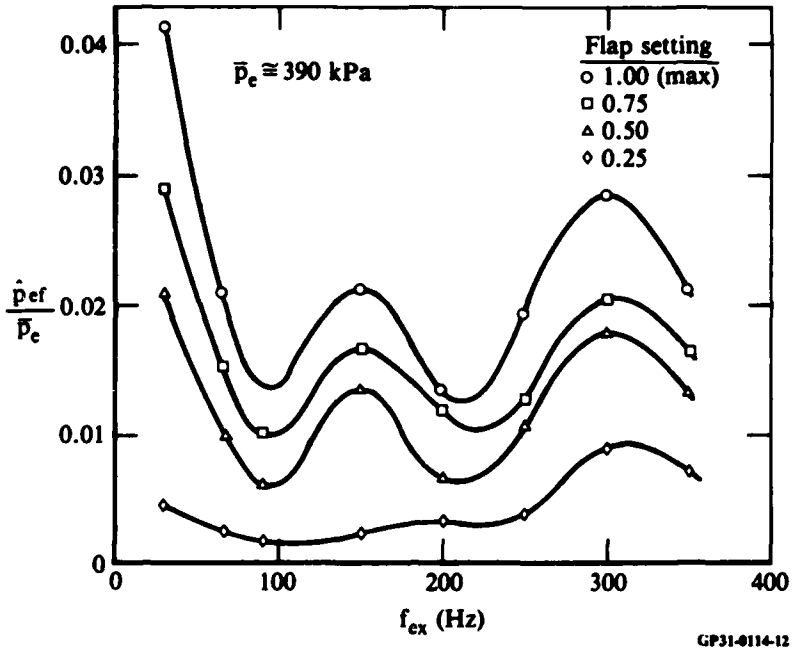

Figure 11. Dependence of exit amplitude on excitation frequency for four different flap settings. $\tilde{M}_e = 0.420$.

The difficulties were greatly alleviated by the fact that the internal (wall) pressure perturbation amplitudes varied linearly with the exit amplitude. This linearity is illustrated in Figure 12. Data taken at the same excitation frequency fall closely on a straight line: the correlation coefficients for least-squares fit straight lines were typically over 0.99. Linear behavior was found for all supercritical conditions, for all frequencies/amplitudes, and at all locations where the flow was subsonic at all times. Linearity failed only at those locations that were intermittently passed over by the shock during its downstream excursions.

The slope of the linear relations (P) is actually the local wall pressure amplitude normalized by the exit pressure amplitude. P depends on $\tilde{M}_e$ and the excitation frequency but not on the exit amplitude, which was effectively eliminated as a variable by normalization. The number of independent variables for this class of oscillations is thus reduced from three to two.

Figure 13 contains curves of normalized wall pressure as a function of frequency for transducer T3 ($\tilde{x}$ = 5.76), which is downstream of the shock. Data for four $\tilde{M}_e$ values are given. The symbols are test results, while the

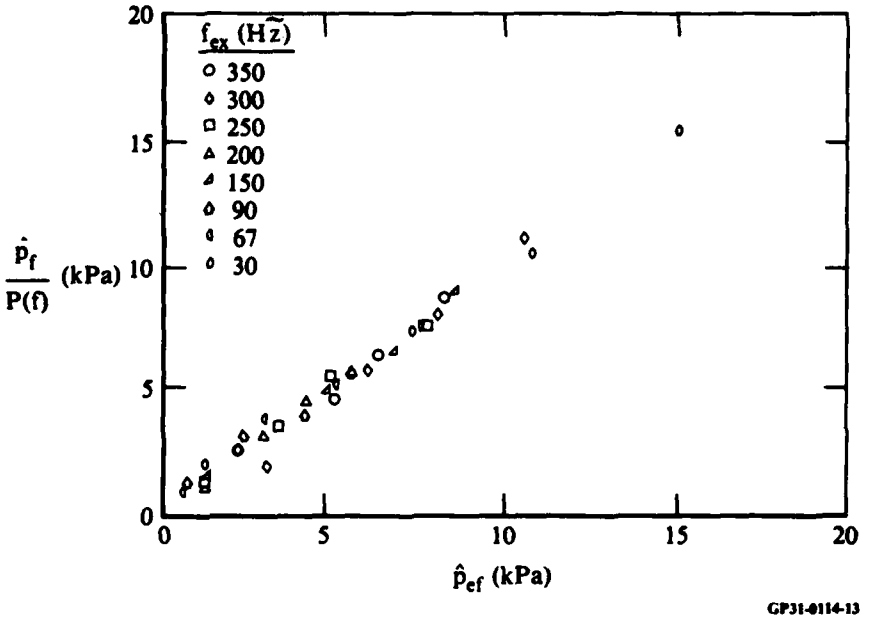

Figure 12. Linearity of induced wall pressure fluctuation amplitudes for $M_e = 0.410$ and $\bar{x} = 5.76$.

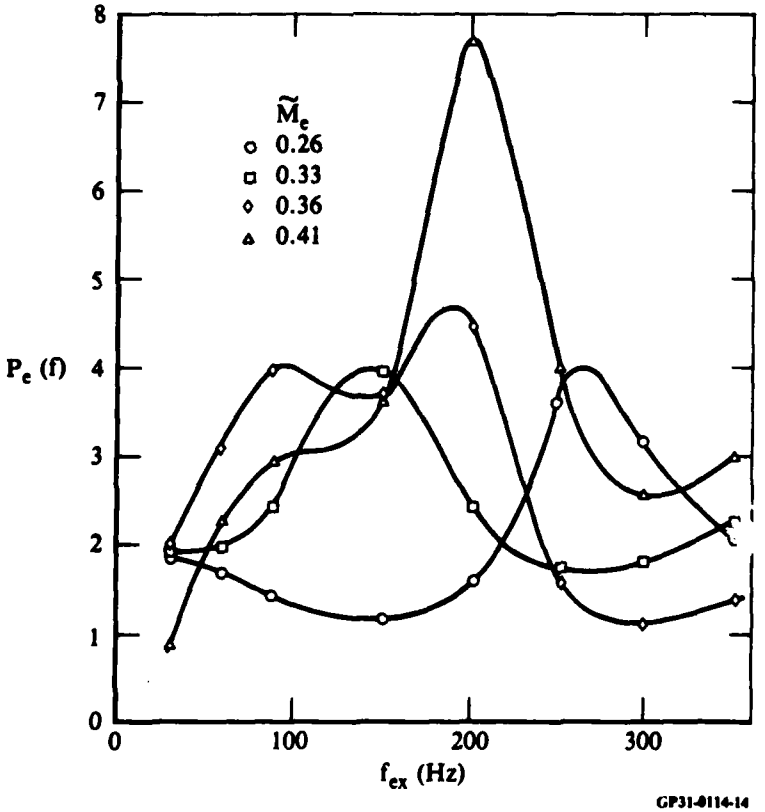

Figure 13. Normalized wall pressure fluctuation amplitudes at $\bar{x}$ = 5.76 for four flow conditions.

lines are somewhat conjectural indications of what the behavior is thought to be between the test points. The curves indicate a strong frequency dependence, even if conservative error bands are superimposed.

The curves of Figure 13 were used to construct the contour plot of Figure 14, which includes additional interpolations with respect to $\tilde{M}_e$. Similar contour plots were prepared for three other transducer locations ($\tilde{x}$ = 7.37, 8.99, and 13.83), all of which were found to have nearly identical structures. It is therefore probable that the contour plot of Figure 14 reflects actual trends, despite the smoothing and interpolation employed. The following trends are recognized:

- At a near-critical condition ($\tilde{M}_e$ = 0.27), the normalized wall pressure amplitude peaks at approximately 280 Hz. This peak frequency gradually decreases to 150 Hz as $\tilde{M}_e$ is increased to 0.33.
- As $\tilde{M}_e$ is increased above 0.33, two well-defined peaks emerge, one at 90 Hz and another at 190 Hz. These peak frequencies stay approximately constant up to the experimental limit of $\tilde{M}_e$ = 0.41.

To the best of the authors' knowledge, the present results constitute the first experimental demonstration of linearity of the response of such a complex flowfield to relatively large perturbations. Acoustic theories assume such linearity, but the amplitude limitation on the assumption is always a question. In the present model, linear response was found at exit amplitudes up to 7.5% of the mean exit static pressure. The largest observed internal pressure amplitude was approximately 16% of the exit static pressure (occurred at conditions other than those causing the previously mentioned 7.5% exit amplitude).

Demonstration of the linear system response and determination of flow conditions associated with peak sensitivity were made possible by the variable-amplitude feature of the exciter mechanism, fully justifying the considerable effort expended in its development.

7.2 Buzz with Excitation

Forced oscillations at sub- or noncritical mean flow conditions invariably involved periodic changes of criticality states and are therefore classified as buzz. Dual and triple buzz both occurred (Figure 10).

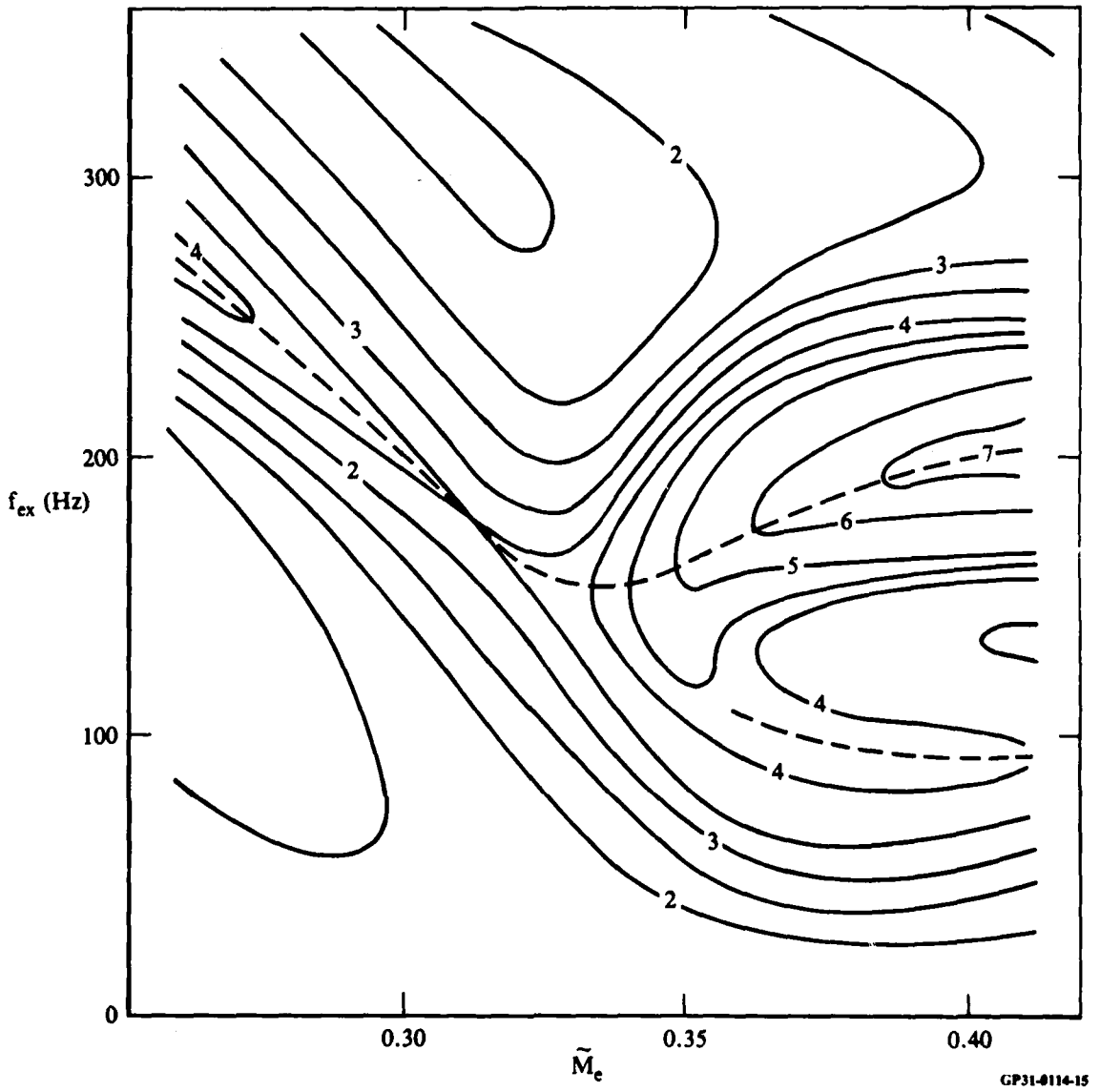

Figure 14. Contour plot of normalized pressure fluctuation amplitudes (P) at $\tilde{x}=5.85$, contours at increments of 0.5. Dashed lines indicate frequencies for maximum response.

Triple buzz displayed greater shock motion amplitudes than dual buzz, but the differences between the two types were not as marked as they were without excitation. Excitation moved the mean shock position downstream, on occasion changing a triple mode into a dual one by eliminating the noncritical portion of the oscillatory range. The similarities allow joint discussion of the two modes of forced buzz.

The case of $\tilde{M}$ = 0.180 with fixed maximum flap setting was selected for detailed study. At this condition the unexcited flow displayed full buzz at 64 Hz. High-speed movies and top-wall static-pressure fluctuation power spectral density distributions (PSD's) were obtained without and with excitation at several frequencies. Attention was focused on transducer T2, located at $\tilde{x}$ = 4.15, a location sufficiently downstream of the shock to remain subsonic at all times, yet sufficiently close to the shock to assure similarity between pressure and shock displacement spectra at low frequencies.

The spectrum and waveform of the exit pressure in natural buzz, $p_e(t)$, is shown in Figure 15a, b. The fluctuation is clearly dominated by periodic contributions, consisting of several significant harmonics which are also evident from the distorted waveform. Random contributions are negligible.

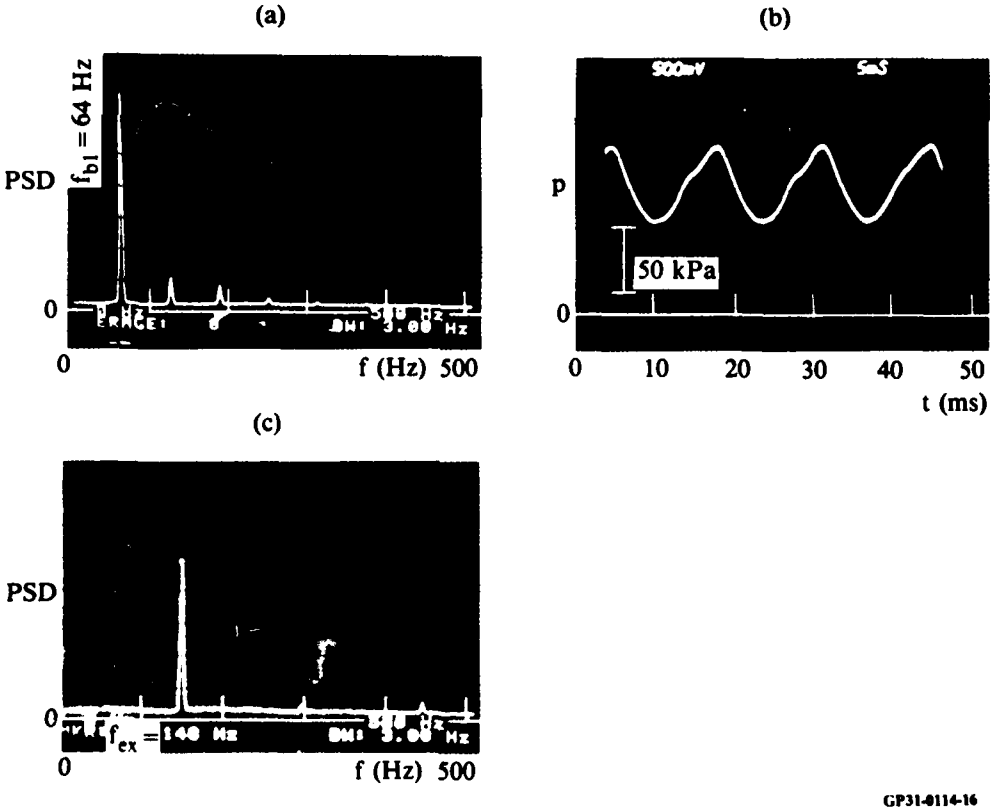

Figure 15. Pressure signals from top wall pressure transducer at $\tilde{x}$ = 4.15. (a), (b) $\tilde{M}_e$ = 0.180, noncritical, unexcited, full buzz; (c) $\tilde{M}_e$ = 0.430, supercritical, excited at 148 Hz.

The perturbation introduced by the exciter cannot be isolated either from natural oscillations or from the response generated by the inlet. As an approximation, the spectrum of $p_e(t)$ for a supercritical flow ($\tilde{M}_e = 0.430$) is shown in Figure 15c. Under this condition, reflections from the terminal shock are presumably weak (Reference 13), and the upstream-moving wave introduced by the exciter is probably the principal contributor to the measured $p_e(t)$. The spectrum is dominated by a sharp peak with small higher harmonics, i.e., the excitation is essentially sinusoidal.

In this class of motions, the natural and forced contributions do not merely coexist, but interact with each other in various complex ways. Figure 16 shows a sequence of spectra obtained at 4 excitation frequencies from 28 to 86 Hz, a range containing the natural buzz frequency (f_{b1} = 64 Hz). The spec-

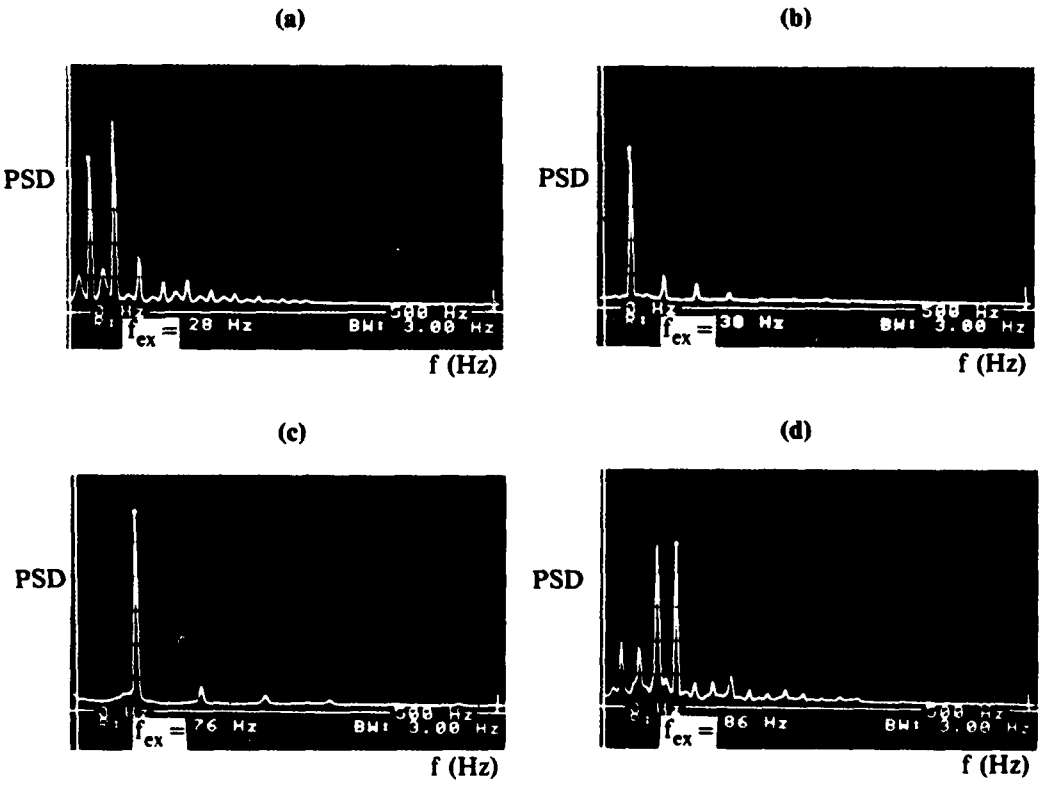

Figure 16. Pressure fluctuation PSD's at $\tilde{M}_e = 0.180$ from top-wall transducer at $\tilde{x} = 4.15$, for frequencies near the 62 Hz natural buzz frequency (f_{b_1}). Note the presence of numerous peaks if excitation frequency (f_{ex}) is far from f_{b_1}. If f_{ex} is close to f_{b_1}, a simple set of harmonics is observed.

tra for f_{ex} = 38 and 76 Hz are similar to the natural buzz spectra (Figure 15a); the only difference is that the fundamental peak occurs at the excitation frequency. High-speed films show little difference between natural and excited flows in these two cases. The spectra for 28 and 86 Hz, however, display a significantly different structure, consisting of many more peaks than either of the two basic spectra (Figure 15a and 15c).

High-speed films of forced buzz in these cases clearly show the presence of many contributory frequencies and the resulting complex wave shapes. Since some of the frequencies may be low, the periods are long, not clearly recognizable, and the motion has the appearance of being random.

Further investigation of these differences revealed that two distinct types of interactions may occur between natural and forced motions; these are discussed in the next two sections.

7.2.1 Modification of Buzz

If the excitation frequency was close to the natural buzz frequency (f_{bl}), then the resultant motion was similar to unexcited buzz; it merely occurred at f_{ex}, at larger amplitudes. The shock position range was displaced downstream, which in some cases changed the mode of oscillation from triple buzz to dual buzz. This modification of the natural mode occurred over the frequency range

$$0.5 \lesssim \frac{f_{ex}}{f_{bl}} \lesssim 1.3 \qquad (3)$$

and is illustrated by the 38 and 76 Hz cases in Figure 16.

Modification also occurred when f_{ex} was close to a higher harmonic of f_{bl}, although the frequency range for such coupling was increasingly narrower for higher harmonics. In such cases the fundamental frequency was a submultiple of the excitation frequency

$$f_1 = f_{ex} / n, \quad n = 2, 3... \ .$$

f_1 was always close to, but not necessarily equal to, f_{bl}. Figure 17 illustrates such forced buzz spectra for the n = 2, 4, 5, and 6 cases.

If modification occurs at the n^{th} submultiple of f_{ex}, then the amplitudes of the n^{th} peak and of the fundamental both increase, while the other peaks remain largely unaffected. Furthermore, the greatest amplitude always occurs at the fundamental, regardless of which harmonic couples to the excitation frequency. This observation indicates a transfer of energy among harmonics, which is a typically nonlinear phenomenon.

7.2.2 Modulation

If the excitation frequency is not close to the natural buzz frequency or one of its harmonics, then a different type of interaction takes place: the excitation modulates the buzz (for $f_{ex} < f_{bl}$) or the buzz modulates the excitation (for $f_{bl} < f_{ex}$).

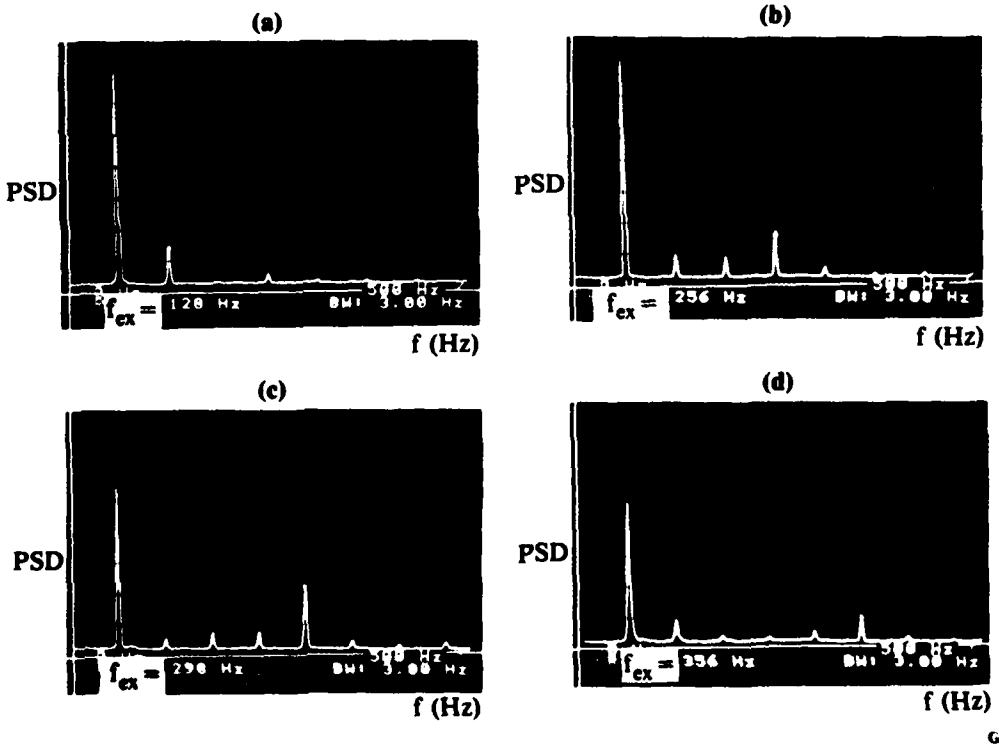

Figure 17. Modification of buzz frequency by coupling between the excitation frequency and a higher harmonic (m = 2, 4, 5, 6) of the buzz frequency. $M_e = 0.180$, $\bar{x} = 4.15$.

Figure 18 shows the PSD for the case where f_{ex} is between f_{b3} and f_{b4}. The natural buzz pattern ($f_{bn} = nf_{b1}$, n = 1, 2, 3...) appears with the peak representing the excitation ($f = f_{ex}$). In addition, a number of new peaks appear, whose frequencies are found to be given precisely by

$$f_j = |f_{ex} \pm jf_{b1}|, \; j = 1, 2, 3... , \tag{4}$$

i.e., the frequencies are given as the absolute values of the sums and differences of the excitation frequency and the buzz harmonics.

The origin of these frequencies can be found by considering the trigonometric identity,

$$2 \cos (2\pi f_{ex} t) \cos(2\pi j f_{b1} t) = \cos[2\pi(f_{ex} - jf_{b1})t] + \cos[2\pi(f_{ex} + jf_{b1})t], \tag{5}$$

from which it is evident that the measured waveform can be described as a product of two basic waves. One basic wave is related to the excitation,

$$p_{ex}(t) = 1 + E_1 \cos(2\pi f_{ex} t) , \tag{6}$$

and the other describes the buzz and its harmonics,

GP31-0114-19

Figure 18. Modulation of buzz by excitation. $M_e = 0.180$, $\tilde{x} = 4.15$.

$$p_b(t) = \sum_{j=1}^{6} B_j \cos(2\pi j f_{b1} t), \qquad (7)$$

where E_1 and B_j are constant coefficients.

The process of generating a new wave by multiplying two basic waves is called modulation of the higher-frequency wave by the lower-frequency one. In some cases, sidebands occur on both sides of the excitation peaks (Figure 19) that are reminiscent of spectra discussed in amplitude-modulated radio transmission technology.

Examples of modified and modulated pressure signals are compared in Figure 20. The modified wave shows the evidence of higher harmonics, but it is dominated by the fundamental. Successive waveforms are repeated for each fundamental period. The modulated wave shape is much more complex, in part due to the fact that there are buzz harmonics both below and above the excitation frequency, and there is no clearly defined carrier wave. The essential feature (that the measured wave is a product of two other waves) can only be verified from the PSD's.

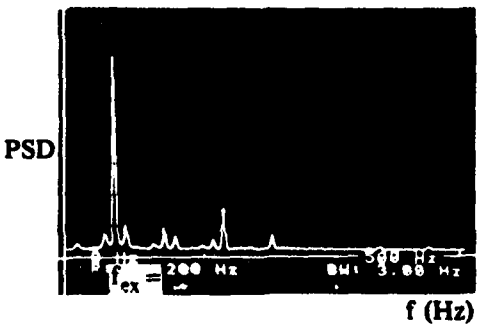

GP31-0114-20

Figure 19. Illustration of sidebands introduced by modulation, $M_e = 0.180$, $\bar{x} = 4.15$.

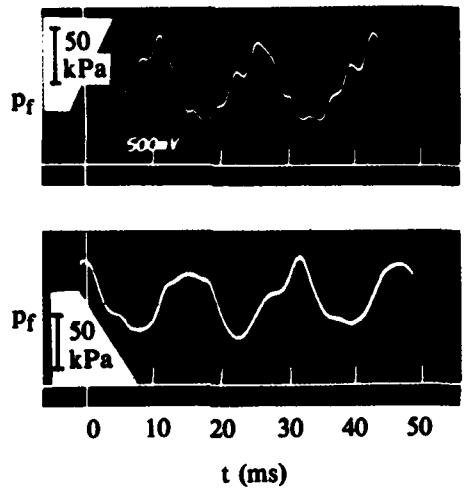

Figure 20. Modified and modulated waveforms, $M_e = 0.180$, $\bar{x} = 4.15$. (a) $f_{ex} = 346$ and (b) $f_{ex} = 150$.

7.2.3 Linearity

The discussion of the previous sections clearly indicates that both types of forced buzz are highly nonlinear phenomena. Linear amplitude response, which so conveniently simplified the description of purely supercritical oscillations, is not expected. Even if it were found, it would be accidental since no linear theory can describe the observed spectral transfer of energy and/or the amplitude modulation observed.

Correspondingly, no attempt was made to establish the response vs. excitation amplitude characteristics in this mode.

8. CRITICALITY BOUNDARIES

8.1 Procedures

Passage of the terminal shock over the cowl or the ramp lips was detected by fast-response pressure transducers located on the outside of the cowl and ramp surfaces, i.e., on the downstream walls of the large suction slots separating the nozzle from the inlet (Figure 3). For supercritical conditions, the transducer signals contained low-level noise only (Figure 21a), while entry into the subcritical state produced disturbances in the cowl slot signal, illustrated in Figure 21b. Entry into the noncritical state was invariably associated with full buzz and the abrupt appearance of square-wave like signals from the ramp slot transducer (Figure 21d).

The boundaries were approached by gradually closing the doors while keeping excitation frequency and flap position constant. The slot transducer

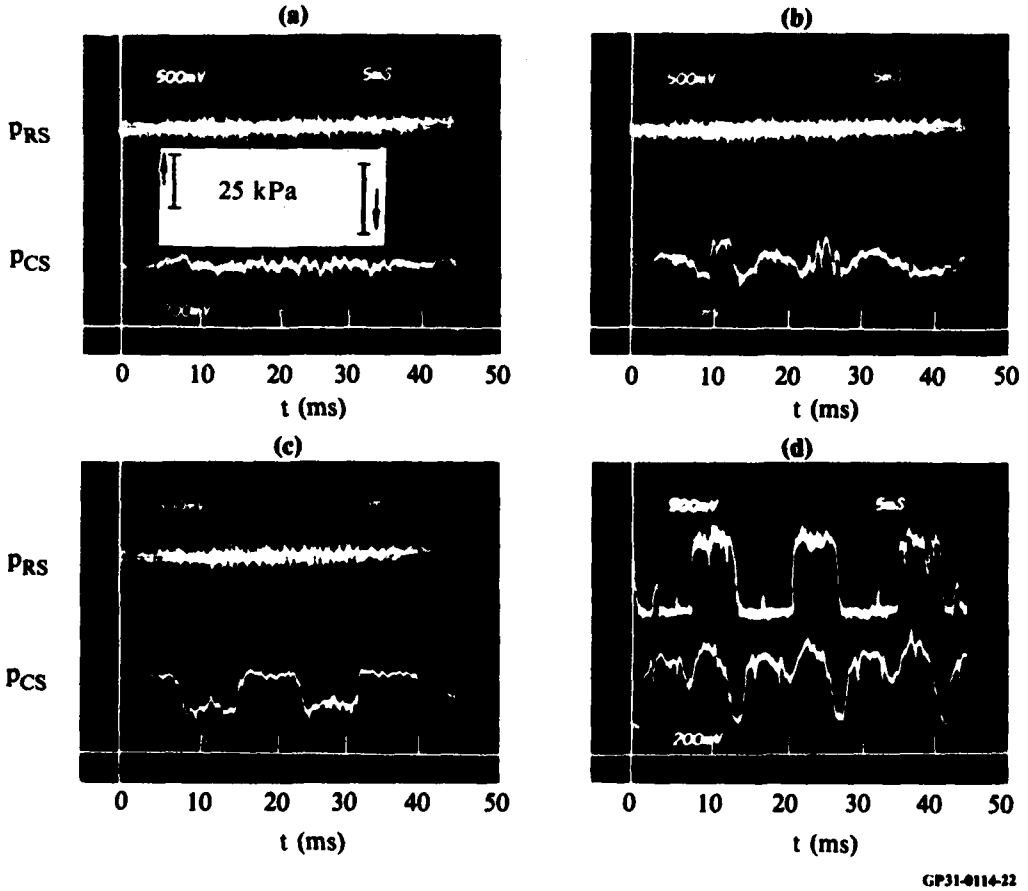

Figure 21. Pressure traces from transducers located in ramp slot (RS) and cowl slot (CS). (a) Supercritical, (b) critical, (c) subcritical, and (d) noncritical (full buzz).

signals were monitored visually during the process; the first appearance of perturbations indicated that the boundary condition had been reached. The door-closing process was associated with variations of the excitation amplitude, $\hat{p}_{ef}$, so that the value of $\hat{p}_{ef}$ associated with the boundary was a test result rather than a controlled variable.

Figures 22, 23 and 24 illustrate the boundaries. Figure 22 shows the limiting $\tilde{M}_e$ values as a function of frequency for four different flap positions, and Figures 23 and 24 show the $\tilde{p}_{ef}$ values measured at the boundaries in the same test series. All symbols are experimental data. Data taken with the same flap settings are connected by straight lines for easier visualization.

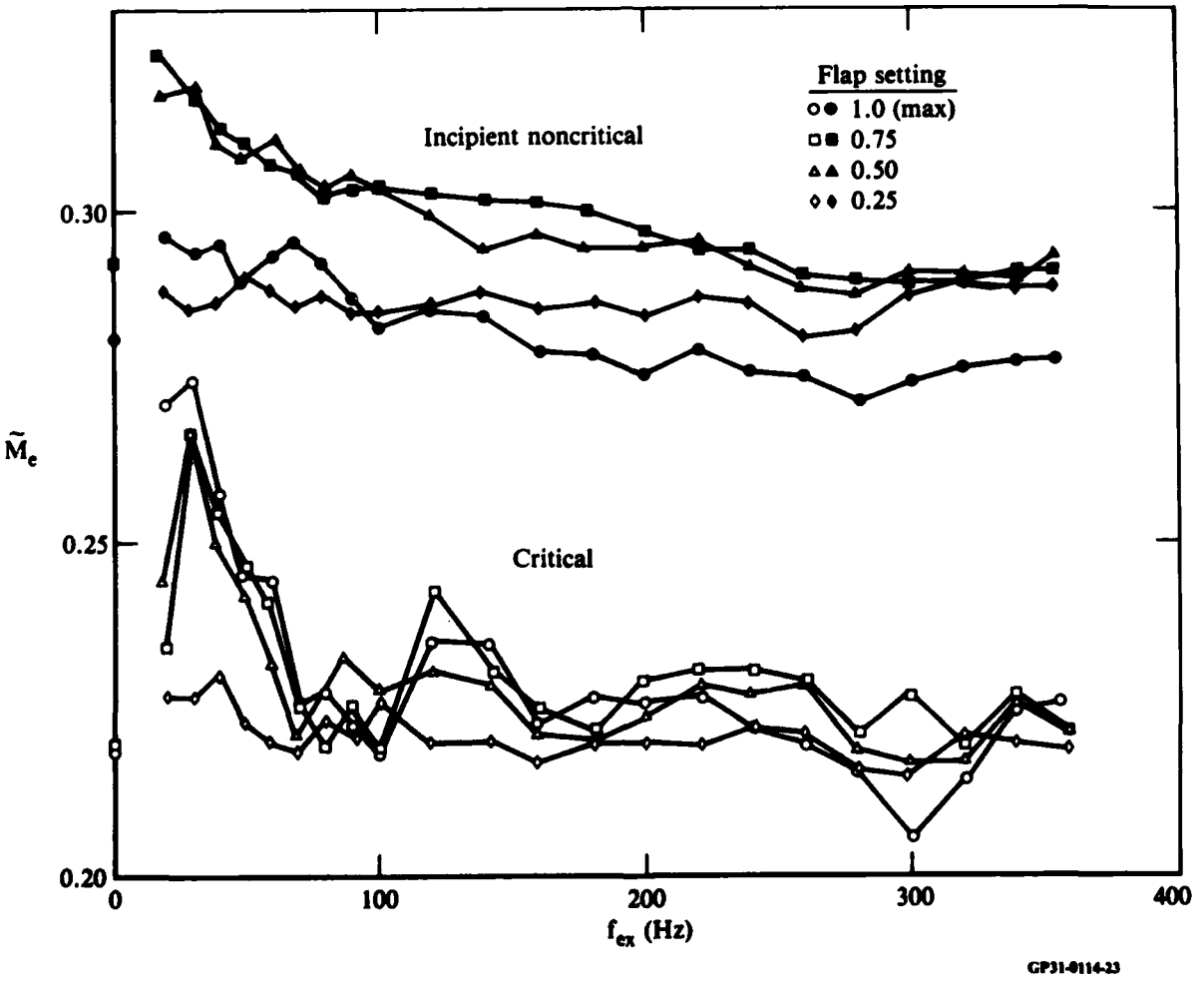

Figure 22. $\tilde{M}_e$ as a function of f_{ex} for various flap settings at the critical and the incipient noncritical boundaries.

Figures 22, 23 and 24 represent the experimental information available in a form closely related to the experimental procedures. For interpreting the results, the flap setting is of no importance and was eliminated by combining the two figures to produce plots of $\tilde{M}_e$ values as a function of excitation intensity and frequency (Figures 25 and 26). These figures contain only operational parameters of direct concern, at the cost of somewhat reduced precision introduced by the interpolations needed in the cross-plotting procedure.

8.2 Discussion of Criticality Boundaries

Figures 25 and 26 represent the boundaries referred to in Section 2 (Task III) and more precisely defined in Section 5.6. They represent perhaps the most useful engineering information in this report.

The shape of the explored ($\hat{p}_{ef}$, f_{ex}) domain is irregular in each case, because the maximum $\hat{p}_{ef}$ value obtainable by keeping the flaps at maximum setting was a strong function of f_{ex}. The domain shape thus reflects experi-

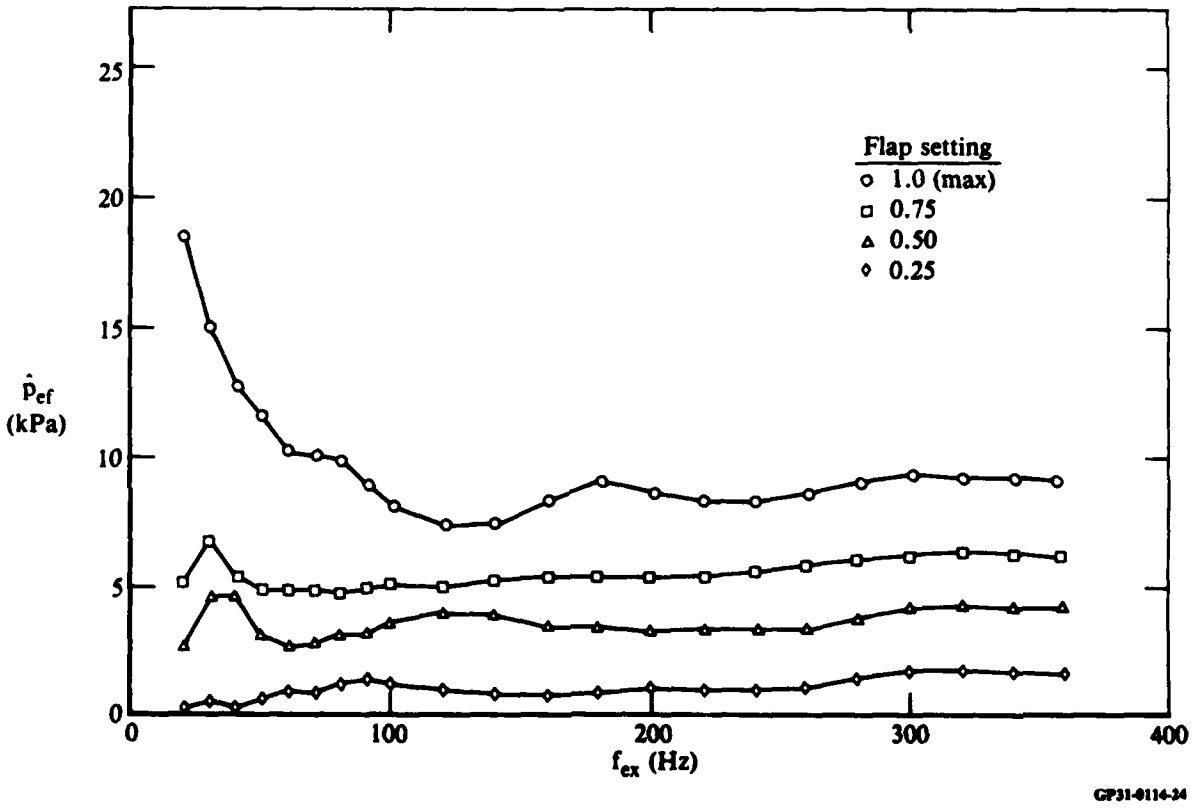

Figure 23. $\hat{p}_{ef}$ as a function of f_{ex} for various flap settings at the critical boundary.

mental limitations only and is therefore largely irrelevant. Given time and resources, the boundaries could be determined, in principle, for additional regions of the $\hat{p}_{ef}(f_{ex})$ plane.

The important information is contained in the values of $\tilde{M}_e$ which is proportional to the degree of supercriticality. Higher $\tilde{M}_e$ indicates that a higher margin is required to prevent reaching the critical boundary (CB) or the incipient noncritical boundary (INB). Since the INB is also the boundary for the onset of full (triple) buzz, INB is probably the more important of the two.

A dominant feature shared by the two boundaries is the rapid increase of $\tilde{M}_e$ as frequencies decrease below approximately 75 Hz. This frequency corresponds to the upper limit at which the excitation can couple to the buzz fundamental (Section 7.2.1). Frequency dependence is weak above 75 Hz.

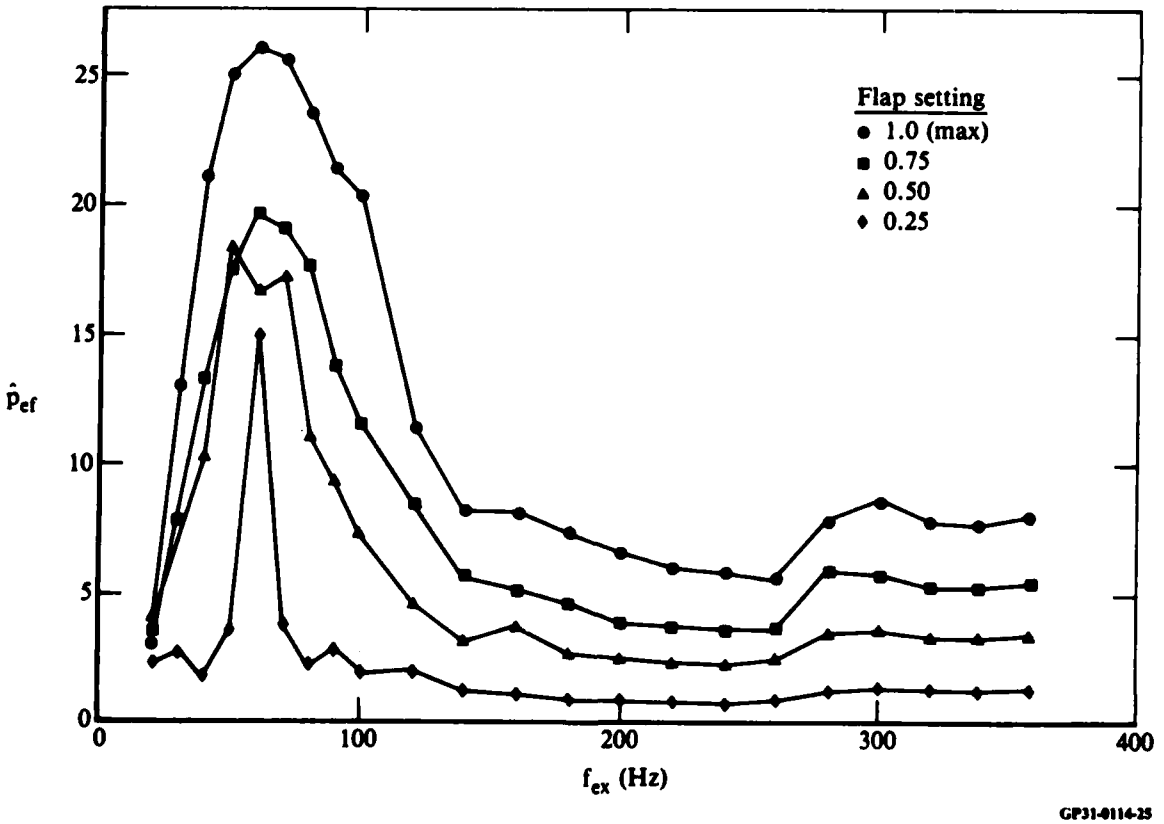

Figure 24. $\hat{p}_{ef}$ as a function of f_{ex} for various flap settings at the incipient noncritical boundary.

Dependence on exit amplitude is different for the two boundaries. For the CB, the $\tilde{M}_e$ value at the boundary peaks at $\hat{p}_{ef} = \cong 5$ kPa regardless of frequency. This feature is puzzling since the expectation is that $\tilde{M}_e$ should increase monotonically with $\hat{p}_{ef}$: increasing excitation amplitudes will be associated with increasingly greater shock displacements, and, since the upstream-most position (minimum x_σ) is held fixed at the cowl or the ramp, the mean shock position will move downstream. In the absence of excitation, such a position is associated with stronger shocks, higher losses, and a higher exit Mach number. The experimental trend for $\hat{p}_{ef} > 5$ kPa is the opposite of this expectation. One possible cause of this anomaly might be the reduction of subsonic viscous losses with increasing oscillation amplitude, as already mentioned in Section 7.

The amplitude dependence of the INB (Figure 25) differs considerably from that found in the CB. The INB displays little amplitude dependence above the buzz frequency, but below it, $\tilde{M}_e$ increases sharply and linearly with $\hat{p}_{ef}$. In combination with the already described frequency dependence, the low-frequency/high-amplitude combination is clearly the most likely to cause the inlet to reach the INB and thereby the onset of full buzz.

The subcritical conditions immediately adjacent to the INB correspond mostly to dual buzz mode oscillations, with the exception of low amplitudes and certain narrow $\tilde{M}_e$ ranges in which pure subcritical oscillations may occur. As explained in Section 7.2, the excitation may either modulate or modify the natural buzz. The ranges for each type of coupling have not been explored in sufficient detail to allow their graphic delineation to be superimposed on Figure 26. However, the absence of any kind of anomaly from the boundaries at any of the higher buzz harmonics shows that excitation at some multiple of the buzz frequency is ineffective and does not demand an increase of margin to maintain stable operation.

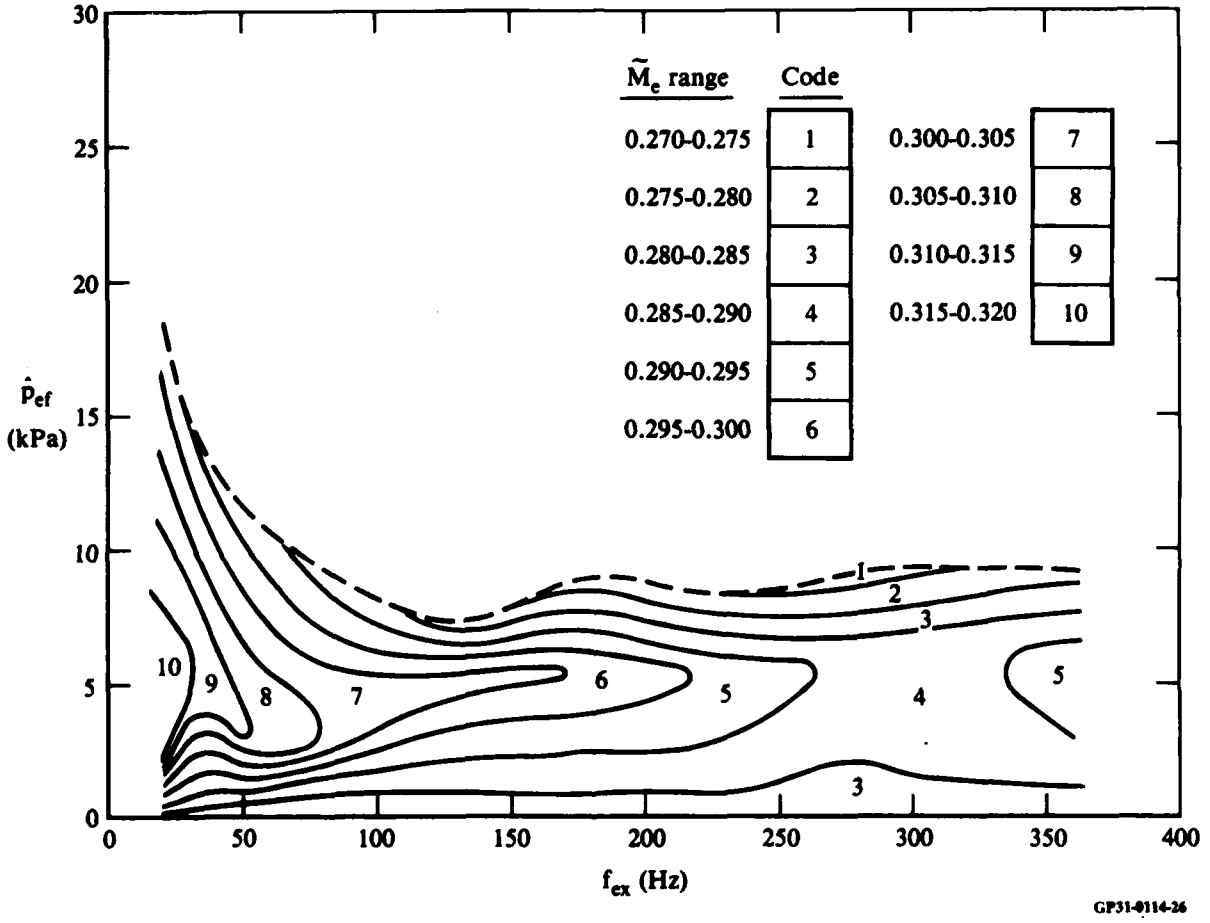

Figure 25. Critical boundary separating supercritical and subcritical flow conditions in the presence of excitation. Upper edge of explored region corresponds to maximum flap setting.

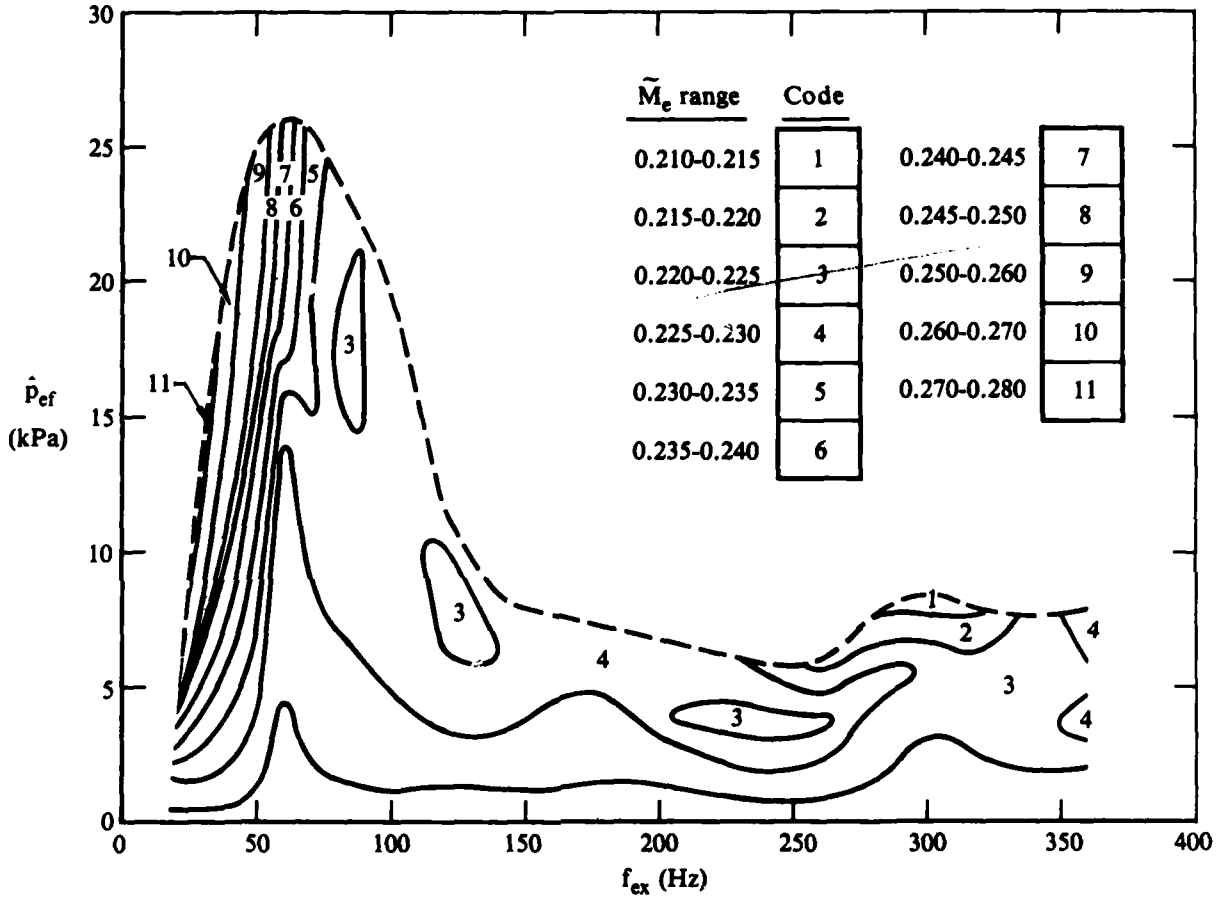

GP31-0114-27

Figure 26. Incipient noncritical boundary separating subcritical and noncritical flow conditions in the presence of excitation. Upper edge of explored region corresponds to maximum flap setting.

9. SUMMARY

The response of an external-compression, M_∞ = 1.84 inlet to periodic downstream perturbations was explored experimentally over all ranges of criticality. The peak-to-peak amplitude of the exit-station pressure fluctuations ranged up to 8% of the mean exit pressure at frequencies from 20 to 360 Hz. The findings are described using a set of terms defined to be valid in the presence of natural or externally induced unsteadiness.

In pure supercritical oscillations, the natural fluctuations are broadband and do not appear to couple strongly to the enforced periodic motion. The amplitudes of internal pressure fluctuations in the subsonic region (filtered at the excitation frequency) vary linearly with the exct amplitude under all supercritical conditions. The response depends strongly on frequency and on mean flow conditions, and distinct frequencies of maximum sensitivity were found.

Subcritical and noncritical conditions are associated with natural oscillations at well-defined discrete frequencies, with minor contributions from random (turbulent) fluctuations. Downstream perturbation at frequencies close to the natural mode will cause the natural mode to occur at the excitation frequency. If the natural and forcing frequencies are too far apart, then the observed pressure vs. time waveforms are precisely described as the product of the excitation waveform and the natural oscillation waveform, including higher harmonics of the latter, up to the sixth. The two oscillations modulate each other.

Criticality boundaries, defined as sets of flow conditions separating the supercritical/subcritical and the subcritical/noncritical flow condition ranges, were determined. The time-mean exit Mach number describing each boundary was independent of frequency over 75 Hz and displayed sharp dependences on both amplitude and frequency below 75 Hz.

The investigated flowfields form a heterogeneous group, with large variations of principal features and dominant mechanisms. It is clear that a more thorough investigation is needed focusing on a more narrowly defined class of flows, permitting a better characterization of the physics. The principal accomplishment of the present study is to provide a basis for the judicious selection of meaningful and manageable problems for future inlet flow investigations.

10. ACKNOWLEDGMENT

The authors wish to thank Mr. M. H. Heinz of McDonnell Douglas Astronautics Company-STL for making them aware of the problem area and its similarity to earlier diffuser work at MDRL. The authors also appreciate the support and early guidance from Mr. Patrick H. Hall of the Naval Weapons Center. Valuable comments and advice came from Messrs. Thomas Rogers and Arthur E. Heins of the Marquardt Company. We greatly appreciate the skills of Mr. Natalie Vignati who designed, assembled, and kept in operating condition the complex array of electronic equipment needed for this program.

REFERENCES

1. P. H. Hall, General Ordnance Ramjet Engine - GORJE, Tests of the Inlet/Combustor (U), NWC TP 6068, Aug. 1978 (Confidential).
2. T. Rogers, Ramjet Inlet/Combustor Pulsations Study, NWC TP 6053, Jan 1980.
3. T. Rogers, Ramjet Inlet/Combustor Pulsations Analysis and Test, NWC TP 6155, Feb 1980.
4. W. H. Clark, Static and Dynamic Performance Investigations of Side Dump Ramjet Combustors: Test Summary, NWC TP 6209, Dec 1980.
5. W. H. Clark, Geometric Scale Effects on Combustion Instabilities in a Side Dump Liquid Fuel Ramjet, 19th JANNAF Combustion Meeting, CPIA Publication No. 366, 1982.
6. K. C. Schadow, J. E. Crump, and F. S. Blomshield, Combustion Instability in a Research Dump Combustor: Inlet Shock Oscillations, CPIA Publication No. 347, Nov. 1981, Vol. III, p. 341.
7. J. E. Crump, K. C. Schadow, F. S. Blomshield, and C. J. Bicker, Combination Instability in a Research Dump Combustor: Pressure Oscillations, CPIA Publication No. 347, Nov. 1981, Vol. III, p. 357.
8. R. C. Waugh, R. S. Brown, T. S. Hood, G. A. Flandro, G. C. Oates, and F. H. Reardon, Ramjet Combustor Instability Investigation Literature Survey and Preliminary Design Study, United Technologies Corporation Report No. UTC/CSD-2770-IR-1, Jan. 1982.
9. M. Sajben, T. J. Bogar, and J. C. Kroutil, Experimental Study of Flows in a Two-Dimensional Inlet Model, AIAA Paper No. 83-0176, Jan. 1983.
10. J. T. Salmon, T. J. Bogar, and M. Sajben, Laser Velocimeter Measurements in Unsteady, Separated, Transonic Diffuser Flows, AIAA Paper No. 81-1197, June 1981.
11. M. Sajben, T. J. Bogar, and J. C. Kroutil, Forced Oscillation Experiments in Supercritical Diffuser Flows with Application to Ramjet Instabilities, AIAA Paper No. 81-1487, July 1981.
12. M. Sajben, and J. C. Kroutil, Effect of Initial Boundary-Layer Thickness on Transonic Diffuser Flows, AIAA J. 19, 1386, (1981).
13. M. Sajben, and T. J. Bogar, Unsteady Transonic Flow in a Two-Dimensional Diffuser: Interpretation of Test Results, McDonnell Douglas Corporation Report No. MDC Q0779, March 1982.

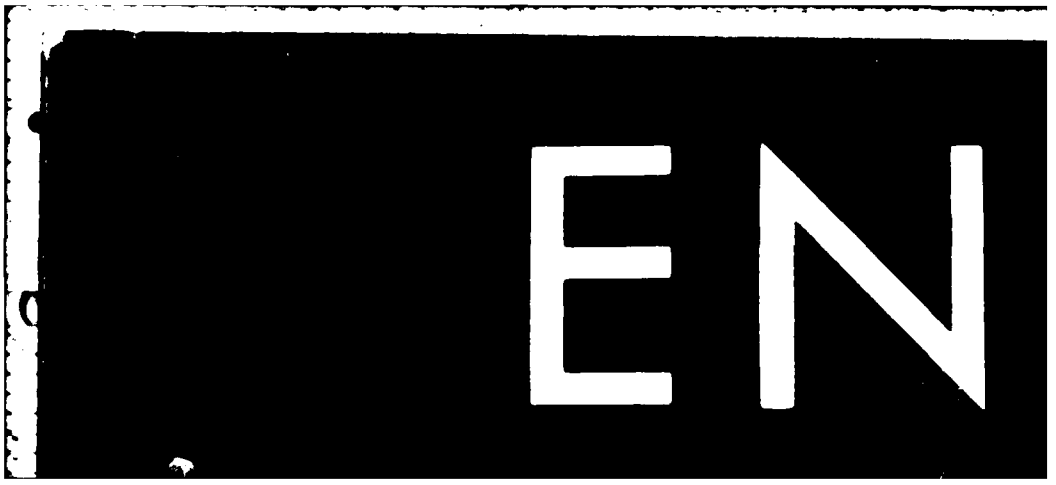
EN